POLITECNICO DI MILANO
School of Industrial and Information Engineering
Master of Science in Aeronautical Engineering
Dipartimento di Scienze e Tecnologie Aerospaziali

Exploratory application of machine learning to damage detection in structural components

Supervisor:

PROF. PIERANGELO MASARATI

Master Thesis by:

JONATHAN ISMANTO
Student Id n. 892278

Academic Year 2018-2019

[July 14, 2019 at 11:48 – version 1.0]

"The noblest pleasure is the joy of understanding."

- Leonardo da Vinci

To my dear parents.

ACKNOWLEDGMENTS

First of all, I would like to thank the advisor of my thesis, Professor Pierangelo Masarati who gave me chance to work on this project, helped and guided me throughout the work. His continuous guidance and assistance helped me in all the time of research and writing of this thesis.

I would like to thank my parents for providing me support, help, and encouragement throughout my years of study. All of this would have not been possible without them.

I express my very profound gratitude to my friends and colleagues who have presented friendly environment during my years in Politecnico di Milano.

Last but not least, I would like to thank Politecnico di Milano for awarding the scholarship for my master study. It has been a wonderful experience to study and meet people from all over the world.

CONTENTS

LIST OF FIGURES

LIST OF TABLES

ABSTRACT

The objective of this work is to detect structural damage in a simply supported beam and helicopter rotor blades. In the simply supported beam, the structural damage is modeled as localized bending stiffness reduction, added mass, and added stiffness in the support. Displacement time-series are obtained from numerical simulation using the free general-purpose multibody solver MBDyn. Multivariable autoregressive model from the displacement time-series is used as the parameter to build the machine learning model. In the helicopter rotor blades, damage due to localized torsional stiffness reduction is simulated. Structural health monitoring algorithm is performed based on strain measurement on the blades. Three algorithms are presented. They use the information from the differences of strain measurement in all of the four blades. Maneuvered flight is also performed to assess the method outside steady flight condition. Mahalanobis squared distance, auto-associative neural network, and singular value decomposition are used as the machine learning algorithms.

SOMMARIO

L'obiettivo di questa tesi è identificare i danni strutturali in una trave e rotore dell'elicottero. Nella trave, il danno strutturale è modellato come riduzione localizzata della rigidezza alla flessione, massa aggiunta e rigidità aggiunta nel supporto. Le serie temporali di spostamento sono ottenute dalla simulazione numerica utilizzando il solver multibody MBDyn. Il modello autoregressivo multivariabile della serie temporale di spostamento viene utilizzato come parametro per costruire il modello di apprendimento automatico. Nel rotore dell'elicottero, viene simulato il danno di riduzione localizzata della rigidità torsionale. L'algoritmo di monitoraggio della salute strutturale viene eseguito sulla base della misurazione della deformazione sulle pale. Vengono presentati tre algoritmi. Viene inoltre eseguito un volo manovrato per valutare il metodo al di fuori delle condizioni di volo stabili. *Mahalanobis squared distance, auto-associative neural network,* e *singular value decomposition* vengono utilizzati per il modello di apprendimento automatico.

1

INTRODUCTION

Science, my boy, is made up of mistakes, but they are mistakes which it is useful to make, because they lead little by little to the truth.

— Verne *Journey to the Center of the Earth* 1957

1.1 STRUCTURAL HEALTH MONITORING

Structural health monitoring (SHM) is the process of implementing a damage detection strategy for aerospace, civil, and mechanical engineering infrastructure (Figueiredo et al., 2010). The process uses measurement from sensors, which can be strain, acceleration, or displacement. Then, the data is analysed to observe the current state and condition of the structure. The tap testing that was performed to detect cracks in railroad wheels in the 1800s is the earliest references to structural health monitoring (Farrar and Worden, 2013).

Damage detection technology for civilian and defence applications in aerospace began during the late 1970s and early 1980s (Farrar and Worden, 2013). In one of the early work, sensors are used to count load cycles. The evolution of structural health monitoring has produced several systems from research to application, which examples are space shuttle modal inspection system (SMIS) and rotorcraft health and usage monitoring system (HUMS). In rotorcraft industry, health and usage monitoring system is implemented on UM-60M Blackhawk helicopter to monitor the main rotor and gearbox components during operation. These systems that use vibration data for predictive maintenance can incrase rotor component life by 15%, reduce the frequency of expensive periodic inspections which is around 25% of the operating cost (Cronkhite, 1993), and increase flight safety. Federal Aviation Administration (FAA) and the Civil Aviation Authority (CAA) have approved the use of HUMS as part of maintenance strategy.

The development of composite materials gives new challenge to the damage detection technology. Composite structures have different behaviour and failure mechanisms, such as delamination and debonding which are not associated with metallic structures. Some constraints on the sensing system are also present, for example weight limitations or composite fuel tank where the sensing systems must not provide a spark hazard. This has led to development of SHM based on fibre optics, active pulse-echo, and pitch-catch wave approaches.

Structural health monitoring for aerospace application is driven by both safety and economic issues. Economic benefits can be obtained if the SHM system reduces the amount of maintenance required, which prevents unnecessary overhaul of the mechanical and structural components. In military application, combat asset readiness of the aircraft can be increased by decreasing the maintenance time.

Data acquisition system is used to sense the states of the system in operating condition. Optical and mechanical (e.g: strain and acceleration) measurement are the most common used. Optical sensors have several benefits which are lightweight, and free from spark hazard. In rotorcraft application, optical sensors have several disadvantages (Serafini et al., 2018). They can only monitor in-sight parts of the object that has sufficient optical markers field. Operation conditions such as the presence of water, ice, or direct sun combined with high speed measurements and vibration lower the performance and accuracy of the measurement. On the other hand, strain measurements are preferred due to its simplicity.

1.2 STATE OF THE ART AND LITERATURE REVIEW

1.2.1 *Multibody system*

Multibody system is a collection of subsystems called bodies, components, or substructures (Shabana, 2005). Different types of joints are used to constrain the motion of the subsystems kinematically. Large translations and rotational displacements may happen in each subsystem or component.

Peaucellier mechanism displayed in figure 1.1 is an example of a multibody system (Shabana, 2005). The mechanism is constructed to create a straight-line path. Due to the constraints BC = BP = EC = EP and AB = AE, points A, C, and P should always arraged on a straight line. In case AD = CD, point C has a circular arc and point P should go on a straight line. This is not the case when elastic deformation of the links is taken into account. If the flexibility is considered, the mechanism can be modeled as a multibody system of rigid and deformable elements.

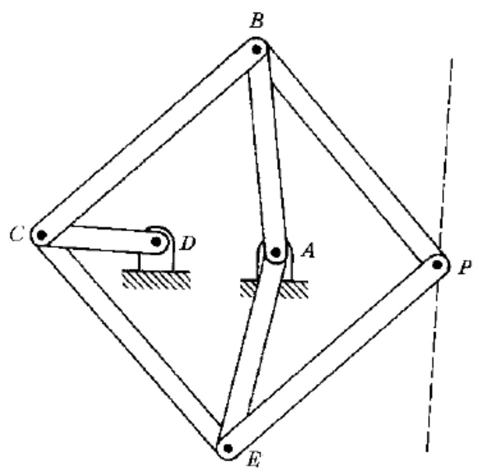

Figure 1.1: Peaucellier mechanism (Shabana, 2005)

The dynamic equations of rigid bodies can be derived by assuming that the rigid body consists of a large number of particles. The unconstrained three-dimensional motion of the rigid body can be described using six equations: three translational equations and three equations of body rotation. Together, they are called Newton-Euler equations, which are expressed in terms of the accelerations and forces acting on the body to characterize an arbitrary rigid body motion.

The Newton-Euler equations for body i in the multibody system can be written as

$$\begin{cases} m^i \dot{v}^i + m^i \omega^i_{\times} v^i = f^i \\ \omega^i_{\times} J^i \omega^i + J^i \dot{\omega}^i = M^i \end{cases} \tag{1.1}$$

where m^i is the total mass of the rigid body, a^i is a vector that defines the absolute acceleration of the center of mass of the body, f^i is the vector of forces acting on the body center of mass, J^i is the mass moment of inertia defined with respect to the center of mass, ω^i is the first derivative with respect to time of the angle that defines the orientation of the body, and M^i is the moment acting on the body.

In multibody systems, the motion of the bodies is constrained because of the mechanical joints, such as revolute, spherical, and prismatic joints. Figure 1.2 shows the example of mechanical joints.

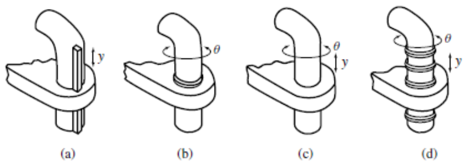

Figure 1.2: Example of mechanical joints. (a) Prismatic or translational, (b) revolute, (c) cylindrical, (d) screw joint (Shabana, 2005)

The mobility of the system is reduced because the motion is no longer independent due to specified trajectories of the mechanical joints. Using a set of nonlinear algebraic constraint equations, the mechanical joints and specified motion trajectories are described. The number of system *degrees of freedom* is defined as the number of the system coordinates minus the number of independent constraint equations. For an n_b rigid body system with n_c independent constraint equations, the number of system degree of freedom is

$$\mathrm{DOF} = 6 \times n_b - n_c \tag{1.2}$$

Figure 1.2 shows some of the commonly used mechanical joints that appear in many mechanical systems. The prismatic or translational joint allows only translation between two bodies. Five kinematic constraints in Cartesian space are used to limit the motion in order to describe the motion only along the joint axis. These equations are constructed by using a set of algebraic equations that impose only relative translation between two bodies along two axes.

The revolute joint allows only relative rotation between two bodies around a revolute joint axis. Five constraint equations are used: three equations that limit relative translation between the two bodies, and two equations that constrain the relative rotation between the two bodies.

The cylindrical joint allows only relative translation and relative rotation between the two bodies along the joint axis.

1.2.2 *Axioms of Structural Health Monitoring*

The study in Structural Health Monitoring has arrived to the point where several fundamental axioms can be written (Farrar and Worden, 2013). Axioms are used to represent the fundamental truth in the methodology.

All material have inherent flaws or defects. It is well known that a perfect periodic structure of a regular lattice of atoms has higher strength than those material samples that are experimentally tested. In the real world, perfect material does not exist, since there are defects at the microstructural level, such as vacancies, inclusions, and impurities. In metals, the presence of microcracks and voids lowers the strength of the material. In composites material, defects also occur at the macrostructural level due to manufacturing processes. These defects drop the strength of the material, therefore the mechanical properties of a specific material are always given as a range of values.

A *defect* is always hidden inside all materials. *Damage* occurs when the structure is not performing in its ideal condition, but possibly in a suboptimal manner. *Failure* happens when the structure is not operating satisfactorily with unacceptable reduction in quality.

Damage assessment requires a comparison between two system states. In the pattern recognition method to structural health monitoring, a training data is required as a baseline. For novelty detection approaches, the training set consists of samples that are obtained from the normal condition of the structure. For higher levels of diagnosis, such as damage type, location, and severity, the training data must contain samples corresponding to various damage conditions.

Identifying the presence of damage can be done in unsupervised learning mode, but identifying the type of damage ans severity can be done in a supervised learning mode. Supervised leaning algorithm learns the data that are obtained from both the undamaged and damaged structures, while unsupervised learning learns only from the undamaged structure. Novelty detection is an example of unsupervised learning application.

In unsupervised learning mode, statistical analysis are used to measure how different is the tested data with the reference undamaged data. Damage sensitive feature extracted from the system response is processed through the algorithm to produce a damage index that can be compared to a predetermined threshold to conclude that damage is present. Basically, this type of learning mode cannot tell the difference between possible type and severity of damage.

In supervised learning mode, the training data consists of data from known types and severity of damage. Finite element model is one of the desired approach to simulate the condition of damage in a structure. In order to have a reliable system, an accurate model of structure must be available. These data can be used to build a machine learning classification and regression models that can indicate the type and level of damage, based on the previously learned data.

Sensor cannot measure the damage directly. It measures the response of the system due to operational and environmental condition. An algorithm is necessary to map sensor data into damage information. As an example, one cannot measure stress directly using a sensor. The measured quantity is the strain which is later mapped to the stress using a certain function. The function depends on the material and geometric properties of the structure.

Using the same analogy, in structural health monitoring with machine learning approach, the function is estimated using known observations from the data. The data can have high dimensionality. In order to have an accurate representation of the model, more training data is needed for increasing amount of dimension of the feature. The first solution is to get enough amount of training sets, which maybe impossible for some situations where the data are limited due to cost and availability constraint. The second approach is to use dimension reduction algorithm to lower the dimension of the data until the available data are enough to make a reliable model. Principal component analysis is one of the example of dimension reduction algorithm.

The measured data depends both on the state of the damage and the environmental and operational condition of the system. Temperature is an example of the environmental condition. Generally, it is desired to find a method to identify the change in damage, with insensitivity from all other sources of environmental and operational variability.

The length and time scales of the phenomena influence the structural health monitoring sensing system. As an example, detection of foreign object impact on an unmanned aerial vehicle needs relatively high sampling rates. Basically, sensor types, number and locations, bandwidth, sampling intervals, data acquisition and systems need to be properly chosen in order to sense the phenomena of the damage condition.

Noise in the measured signal is always present during the measurement process. The reduction of noise allows to have a more accurate reading of the system. The level of noise in the measured data must be reduced as much as possible, which can be performed by various method such as analogue or digital filtering.

The size of damage that can be detected is inversely proportional to the frequency range of excitation. In general, at high frequency range it is easier to see the damage signal differences with the baseline signal.

Damage increases the complexity of a structure. Most of the time, nonlinear response is present in damaged structure. More complex shape needs more information in order to represent it than a simpler pattern. Feature selection is performed by defining the type of damage and its properties.

1.2.3 *Literature review*

Serafini et al., 2019 developed an approach to structural health monitoring of helicopter rotors based on strain measurement on the blade. The algorithms which are based on the analysis of the discrepancies between damaged and undamaged blades.

A mass unbalance at the tip and a localized stiffness reduction are considered in the numerical simulation using multibody dynamic solver for aeroelastic analysis of rotorcraft. Two algorithms are presented: in time domain and in the frequency domain. The first algorithm uses the autocorrelation signal of the discrepancies signal while the second algorithm analyses the discrepancies signal using the power spectral density.

Figure 1.3 shows the autocorrelation, while figure 1.4 displays the power spectral density of the discrepancies signal from damaged (10% stiffness reduction) and undamaged blades.

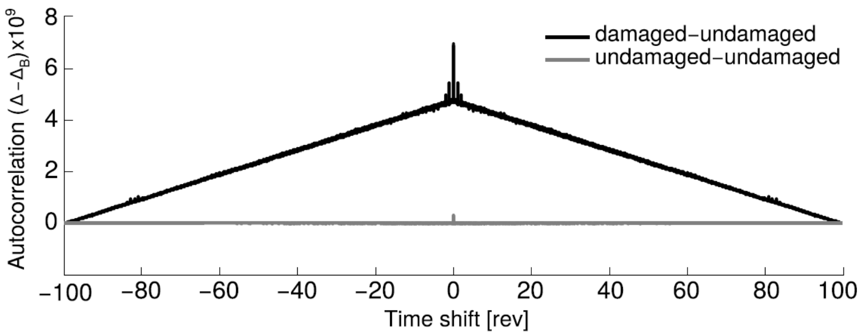

Figure 1.3: Autocorrelation of discrepancies signal from altered (10% flapping stiffness reduction) and nominal blades (Serafini et al., 2019)

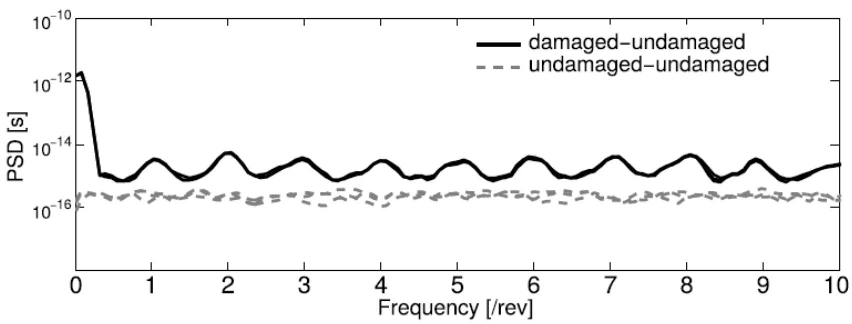

Figure 1.4: PSD of discrepancies signal from altered (10% flapping stiffness reduction) and nominal blades (Serafini et al., 2019)

The methods work better in quasi-steady flight conditions, while the accuracy decreases in aggressive maneuvered flight. Collective excitations of two 1-cos collective doublets are introduced as perturbations.

Figueiredo et al., 2010 applied four machine learning algorithms in order to detect structural damage in presence of operational and environmental variations using vibration. Autoregressive model is used to extract damage-sensitive features from time-series data of accelerometers when the structure is in different state. The algorithms presented are auto-associative neural network, factor analysis, Mahalanobis distance, and singular value decomposition. Each algorithm produces a scalar output which is the damage indicator.

The experimental campaign is performed on three-story frame structure to obtain time-series data from an array of accelerometers under several structural state conditions. The damage is simulated by introducing a bumper mechanism that induces a repetitive impact-type nonlinearity. This mechanism simulates a crack that open and closes under dynamic loads. Figure 1.5 shows the three-story frame aluminum structure used in the experiment.

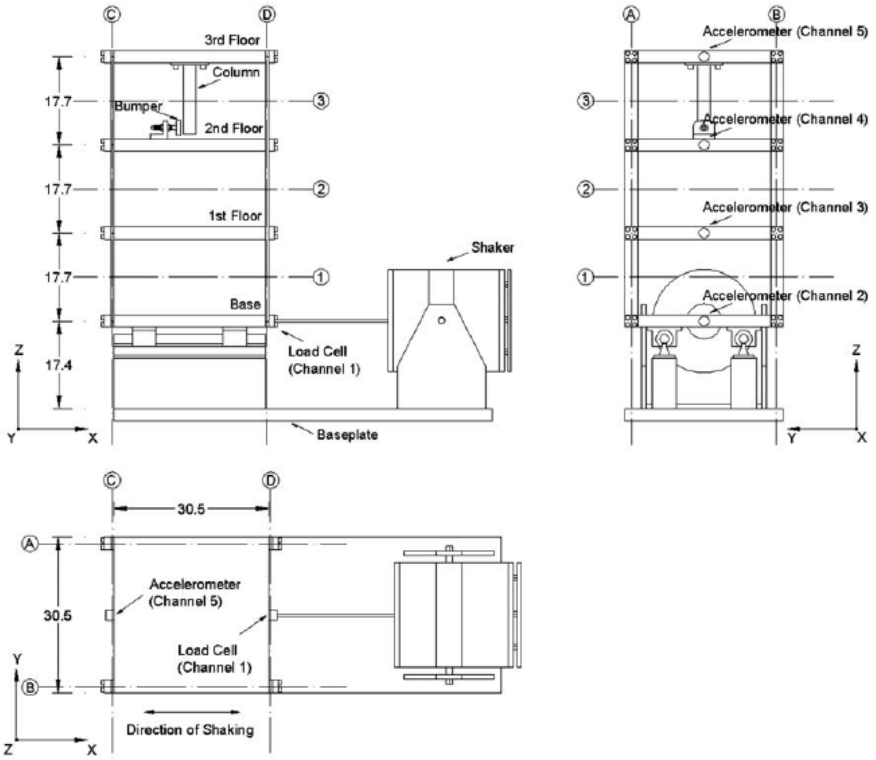

Figure 1.5: Three-story test bed structure (all dimensions are in centimeter) (Figueiredo et al., 2010)

Santos et al., 2015 presented four kernel-based algorithms for damage detection, which are one-class support vector machine, support vector data description, kernel principal component analysis, and greedy kernel principal component analysis. An autoregressive model is built from acceleration time-series measurement from accelerometers. In the test phase, the machine learning algorithm will map each input feature vector into a damage indicator index. The classification is performed using one-sided threshold.

Gul and Catbas, 2009 studied statistical pattern recognition methodologies for structural health monitoring application to detect damages. Outlier analysis from the damage sensitive feature, obtained from autoregressive model is used to detect the changes in the structure. The specimen is a simply supported steel beam, displayed in figure 1.6. The time-response data is obtained by measurement of accelerometers.

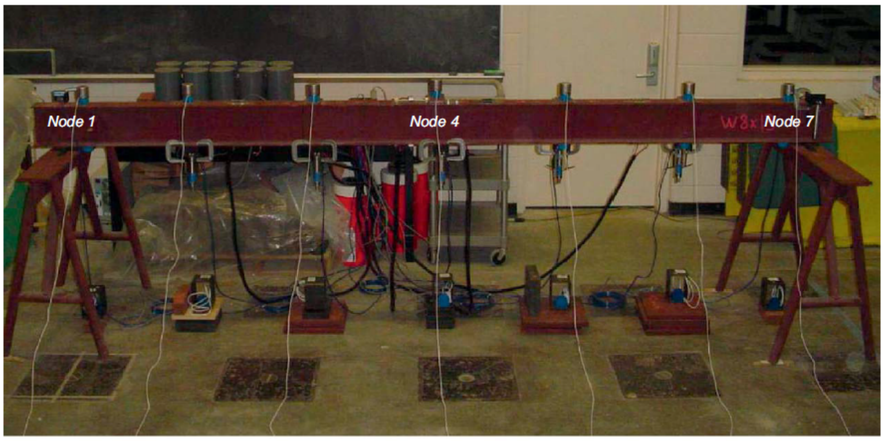

Figure 1.6: The beam test setup (Gul and Catbas, 2009)

The algorithm uses a modified methodology by applying the random decrement method for normalizing the ambient vibration data. Then, autoregressive model of the free responses are constructed. The coefficients of the Autoregressive model are selected as the damage sensitive features. Finally, the condition of different structures are separated by implementing the Mahalanobis distance-based outlier detection algorithm.

Three damage scenario are presented. The first is a case where a pile loss is simulated by removing the roller support between the grid and the column. The second damage case, restrained supports, is simulated by fixing the end supports to create rigidity caused by different phenomena such as corrosion. The third case simulates local stiffness reduction where a connection plate is removed from the structure.

Comparative analysis shows that using random decrement gives better separation during the outlier detection process. The methodology gave successful results, but some of the cases did not show successful result, such as the reduced stiffness case.

Ruotolo and Surace, 1999 used singular value decomposition for detecting damage in structure. The damage detection method is based on the determination of the rank of a matrix. A numerical truss structure is used to validate the damage detection algorithm, shown in figure 1.7. The stiffness of element 4 in figure 1.7 is reduced to 10%, 30%, and 50%.

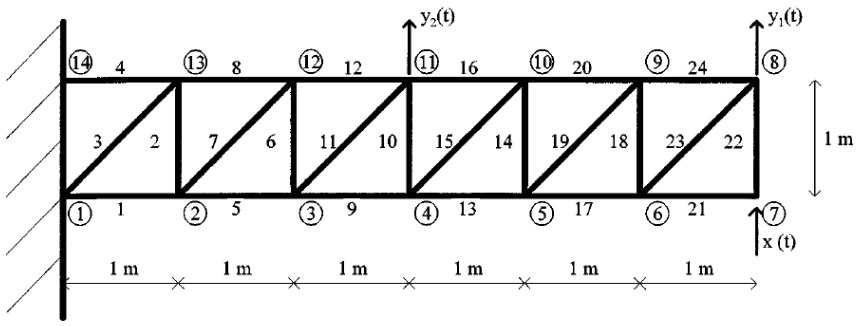

Figure 1.7: The beam test setup (Ruotolo and Surace, 1999)

Amplitude of the frequency response functions are used to build the characteristic vectors. Noises generated from Gaussian distribution with standard deviation equal to 10% of the mean is introduced to the characteristic response function. The result shows that the increasing damage index enable the damage to be detected.

Experimental tests are also performed to a cantilever beam, illustrated in figure 1.8. Three conditions are simulated: concentrated mass not connected to the beam, the lighter mass connected close to free end, and the heavier mass connected close to the free end.

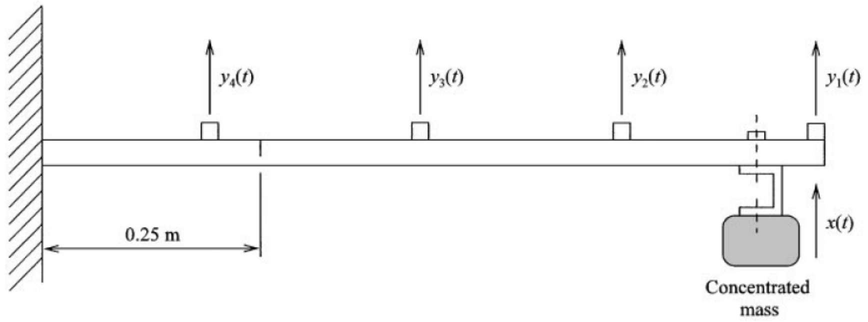

Figure 1.8: The beam test setup (Ruotolo and Surace, 1999)

The frequency response functions are obtained from four sensors for each different conditions. In the end, satisfactory results are obtained.

1.3 OBJECTIVE

In this work, damage detection algorithm is implemented to two different problems, which are simply supported structure and helicopter rotor blades. The simulations are performed numerically using multibody dynamic solver MBDyn.

In the simply supported beam case, several types of damage are considered, which are localized stiffness reduction, added mass, and added stiffness in one of the support. The measurement of displacement in two location on the beam is simulated using multibody solver MBDyn. Multivariate autoregressive model is fitted to the time-series displacement in order to identify the characteristic of the free response signal. Then, Mahalanobis squared distance is used to distinguish between data coming from damaged or undamaged model.

In the helicopter rotor blade, localized torsional stiffness reduction is introduced as a damage. Strain measurement in the blades are used as to perceive the condition of the system. Three algorithms are presented. They use the information from the differences of strain measurement in all of the four blades. Maneuver is also simulated to assess the methods outside steady flight condition. Mahalanobis squared distance, auto-associative neural network, and singular value decomposition are used as the machine learning algorithms.

1.4 OUTLINE

This article is organized in four parts. The first part is the introduction. The second part describes the modeling and analysis in simply supported beam structure. The third part explains the structural health monitoring process in helicopter rotor blades. The last part concludes the work.

2 SIMPLY SUPPORTED BEAM

Science knows no country, because knowledge belongs to humanity, and is the torch which illuminates the world.

— *Louis Pasteur*

2.1 INTRODUCTION

Structural health monitoring involves installations of sensors to collect valuable data about the structure. Knowledge about the structure can be obtained by observing the sensor data. The information and knowledge gained from the sensor data is then used for evaluation of the integrity of the structure and to schedule maintenance activities.

The goal of this work is to detect the presence of damage in a simply supported beam. In this study, the structure is a simply supported beam with damage in the middle and the simulation is performed using a multibody model, generated using MBDyn. Next, Multivariate Autoregressive model is used to collect damage-sensitive features from time-series of displacement data when the structure is in different condition. Then, Mahalanobis squared distance is used as the machine learning algorithm for data normalization, to model the effect of damage. Afterwards, the machine learning algorithm generates a scalar damage index which should be small when the features are obtained from a reference normal undamaged data. Finally, the scalar damage index is compared to a given threshold to classify the tested system if it is damaged or not.

Several types of damage are introduced to the system: bending stiffness reduction, added mass, and added stiffness in the support. They are intended as the effects on the response of an actual damage. The bending stiffness reduction is simulated by dividing the beam into two parts, connected with a rotational joint and a spring stiffness at the damage location. It is intended to simulate fatigue crack. Added mass in the system simulates an unwanted addition of mass that might happen during the operational life of the system. The added stiffness problem simulates some unintended rigidity at the supports due to various reasons such as corrosion.

2.2 MULTIBODY MODEL

MBDyn is the first and possible the only free general purpose Multibody Dynamics analysis software, released under GNU's GPL 2.1. It has been developed at the *Dipartimento di Scienze e Tecnologie Aerospaziali* of the university *Politecnico di Milano*.

MBDyn features integrated multidisciplinary simulation of multibody, multiphysics systems, including nonlinear mechanics of rigid and flexible bodies (geometrically exact and composite-ready beam and shell finite elements, component mode synthesis elements, lumped elements) subjected to kinematic constraints, along with smart materials, electric networks, active control, hydraulic networks, and essential fixed-wing and rotorcraft aerodynamics. It is developed an used in aerospace (aircraft, helicopters, tiltrotors, and spacecraft), wind energy (wind turbines), automotive (cars, trucks), and mechatronic fields (industrial robots, parallel robots, micro aerial vehicles (MAV)) for the analysis and simulation of the dynamics of complex systems.

Five types of model are used in this work. The first one is an undamaged simply supported beam. The second model is a simply supported beam with a rotational joint and spring stiffness in the middle, which simulates crack. The third model is a whole undamaged simply supported beam, with added mass, located at the middle of the beam. The fourth model is an undamaged simply supported beam with added mass located at the left quarter of the beam. The last model is a simply-simply beam with undesired added stiffness at the left support, which simulates unwanted increase of rigidity caused by different reasons such as corrosion (Gul and Catbas, 2009).

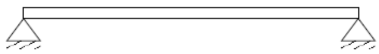

(a) Undamaged beam

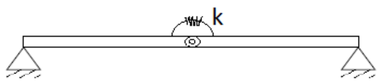

(b) Beam with spring in the middle

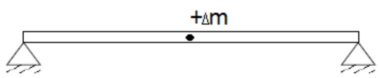

(c) Beam with added mass in the middle

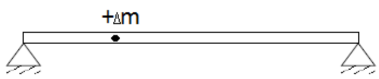

(d) Beam with added mass in the left quarter

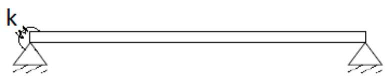

(e) Beam with added stiffness

Figure 2.1: List of the model used in the simulation

The damage in the middle of the beam is simulated using two bodies, connected with a revolute joint and a linear elastic deformable hinge. Two different constitutive laws for the deformable hinge are used. The first one is linear isotropic law, while the second one is nonlinear law. The nonlinear law is implemented to simulate the different behaviour of crack when it is opening or closing. A very high stiffness value is used when the crack is closing and a reduced stiffness value is used when the crack is opening.

The models have 16 beam element, which are built using 3 structural nodes for each element. The nodes at the end of the beam are constrained in translational displacement and are allowed to rotate in one degree of freedom using rotational joint.

The timestep used in the numerical simulation is $\mathrm{dt} = 2 * 10^{-4}\,\mathrm{s}$. It corresponds to sampling frequency of 5kHz. Since the first natural frequency of the problem is around 46Hz, the timestep $\mathrm{dt} = 2 * 10^{-4}\,\mathrm{s}$ is chosen in order to have more than 100 step for each period in the multibody simulation.

The parameters used in model are displayed in table 2.1.

Table 2.1: Beam model's parameters

Parameter	value
Material	
Density [kg/m^3]	2780
Young's modulus [GPa]	73.1
Shear modulus[GPa]	28
Geometry	
Beam's length [m]	1
Beam's thickness [m]	0.02
Beam's width [m]	0.05

In all of the model, two random zero-mean unit force are placed at the middle and the quarter length of the beam from the left support to simulate disturbances to the system. The load time-series are filtered using 2nd order Butterworth's filter with cutoff frequency 400Hz, in order to remove the high frequency loads.

The displacement of the nodes located at $\frac{15}{32}L$ and $\frac{3}{4}L$ from the left support are measured. The location of the damage is in the middle of the beam. Therefore, two measurement from signal close to the damage at $\frac{15}{32}L$ and far from the damage $\frac{3}{4}L$ are used to represent the system.

2.2.1 *Damage simulation*

The simulation of damage is realized as a localized reduction of bending stiffness. Two beams connected with a spring are used. The stiffness profile of a beam with a localized stiffness reduction is equivalent to the presence of spring with an elastic spring.

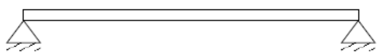

(a) Homogenous beam

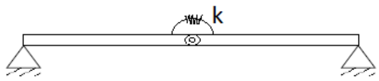

(b) Beam with spring

Figure 2.2: Equivalent beam

The same behaviour is guaranteed if the bending moment M passed through in the discontinuity is equal.

$$M = EIw(\xi)'' = k\Delta w(\xi)' \tag{2.1}$$

where E is the Young's modulus, I is the bending moment of inertia, w is the vertical displacement of the beam, k is the stiffness of the beam, and ξ is the longitudinal axis of the beam.

Figure 2.3 shows the bending stiffness EI in case of stiffness reduction of the homogenous beam with the equivalent beam.

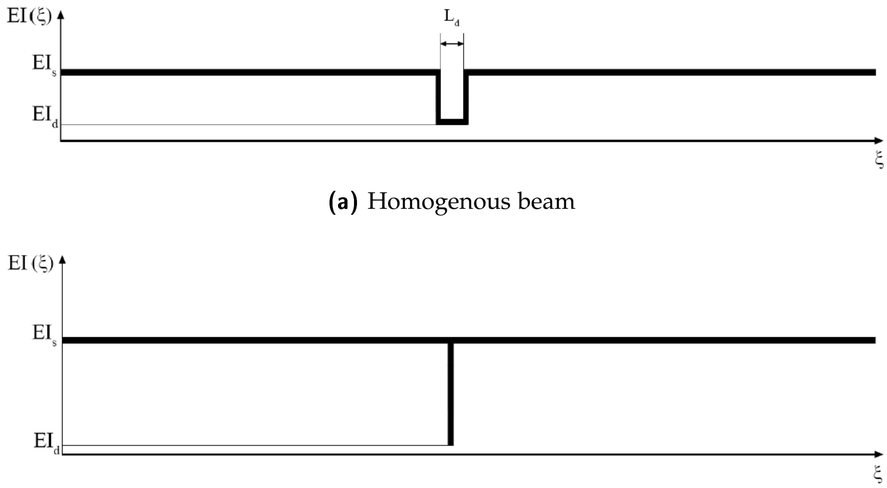

(a) Homogenous beam

(b) Beam with spring

Figure 2.3: Stiffness profile of the equivalent beam

The value of the spring bending stiffness is evaluated by taking into account the equivalence bending angle in equation 2.2.

$$\int_{r-\frac{L_d}{2}}^{r+\frac{L_d}{2}} \frac{M}{S_d} dx = \int_{r^-}^{r-\frac{L_d}{2}} \frac{M}{S_u} dx + \Delta w' + \int_{r^+}^{r+\frac{L_d}{2}} \frac{M}{S_u} dx \, , \tag{2.2}$$

where M, S_u, S_d, L_d are the bending moment, undamaged stiffness, damaged blade stiffness, and length of damage, respectively. Equation 2.2 is solved to obtain the spring stiffness, by assuming constant bending moment in the damaged zone.

Substituting equation 2.1 to equation 2.2 and assuming small L_d, equation 2.3 is obtained.

$$\frac{M}{S_d}L_d = \frac{M}{S_u}L_d + \frac{M}{k} \tag{2.3}$$

The value of k is obtained by solving equation 2.3.

$$K = \frac{\frac{1}{L_d}}{\frac{1}{S_d} - \frac{1}{S_u}} \tag{2.4}$$

2.2.2 *Nonlinear model*

The motivation to implement a nonlinear model is to simulate the nonlinear behaviour of crack under bending load. The crack is simulated using deformable joint with a given stiffness. Its behaviour in stiffness changes depending whether the crack is opened or closed. When the crack is opening, the decreased stiffness value is used, while if the crack is closing, an infinite value of stiffness is applied. The decreased stiffness is obtained as a function of the crack length by using the relation in equation 2.4. For the infinite stiffness, a fixed value of $10^9 Nm/rad$ is used.

The nonlinear constitutive law is implemented in MBDyn by using a continuous contact approach. The nonsmooth nature of contact phenomena is approximated by using a smoothing approximation by a regularization in the description of non-interpenetration and frictional constrains. Stiff repulsion laws take effect when the two members of the system is touching, to represent the non-interpenetrability constraints. The smooth non-impulsive contact force which is a function of local deformability is integrated in the time-steps when contact happens.

Constitutive laws in MBDyn are expressed as $f = f(\epsilon, \dot{\epsilon})$. They define how the resulting force is applied to the model. Different constitutive laws in elements can be implemented in MBDyn without the need to hardcode it. It could be added as a loadable module without altering the base code (Fancello, 2012).

The advantages of this contact model is its simplicity in terms of implementation in multibody analysis. It adds a new stiff contact forces to the Differential Algebraic Equations when contact takes place, then it is integrated by the numerical solvers. The energy dissipation in the collisions can be modeled by adding a damping terms in the constitutive laws.

Several contact force models are available to be used in MBDyn: Flores (Flores et al., 2011) , Hunt Crossley (Hunt and Crossley, 1975), and Lankarani Nikravesh (Lankarani and Nikravesh, 1994). In this work, the model of Flores is used. Flores's contact force model consists of an elastic term and a hysteresis damping parameter that takes into account the energy dissipation phenomena during the contact process.

$$F_N = K\delta^n + K\delta^n \frac{8}{5}\frac{1-e}{e}\frac{1}{\dot{\delta}^-}\dot{\delta} \tag{2.5}$$

F_N is the contact force, K is the stiffness, δ is the deformation of the body, n is the exponent which is a function of the material and geometric configuration. The value is set to $\frac{3}{2}$ in cases where there is parabolic distribution of contact stresses. δ^- is the velocity at the moment of impact, and e is the Newton coefficient of restitution which ranges from 0 to 1. For a perfectly elastic contact, i.e. $e = 1$, the damping term is set to zero, while for a perfectly plastic contact, i.e. $e = 0$, the damping term goes to infinity.

In the crack model, the Newton coefficient of restitution is set to 1 and the stiffness is set to $10^9 \mathrm{Nm/rad}$ to model an infinite stiffness of the deformable hinge when the crack is closing.

2.3 ANALYTICAL SOLUTION AND CONVERGENCE STUDY

2.3.1 *Stiffness reduction in simply supported beam*

It is possible to obtain analytical solution for this simply supported beam problem. By studying the analytical solution, the phenomena of stiffness and frequency reduction due to damage can be observed.

The analytical free vibration problem of the model can be solved by exploiting the symmetry of the structure. Figure 2.4 displays the half model that is going to be analyzed analytically.

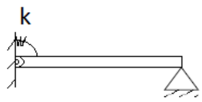

Figure 2.4: Half model

The principle of virtual work for the half model is written as

$$\int_0^{l/2} \delta w'' E J w'' dx + \int_0^{l/2} \delta w m \ddot{w} dx + \delta w'_{(0)} k w'_{(0)} = 0 \quad (2.6)$$

where $w_{(x,t)}$ represents displacement of the beam, E is the Young's modulus, J is the bending inertia, m is the mass per unit length of the beam, and k is the rotational stiffness. Four boundary conditions and one main equation are obtained after integrating by part equation 2.6.

$$EJw'''' + m\ddot{w} = 0 \quad (2.7)$$

Boundary conditions:

$$\begin{cases} w''_{(l/2)} = 0 \\ -EJw''_{(0)} + kw'_{(0)} = 0 \\ w_{(l/2)} = 0 \\ w'''_{(0)} = 0 \end{cases}$$

Assuming solution of $w_{(x,t)} = a_{(x)}b_{(t)}$ and substituting it to equation 2.7, the following equation is obtained.

$$a(x) = A_c\cos(\sqrt{\beta\omega}x) + A_s\sin(\sqrt{\beta\omega}x) + A_p e^{\sqrt{\beta\omega}x} + A_n e^{-\sqrt{\beta\omega}x}\ , \tag{2.8}$$

where $\beta = \sqrt{\frac{m}{EJ}}$. Using $\gamma = \frac{k}{EJ}$, equation 2.8 is substituted to the boundary conditions to obtain a system of equation.

$$\begin{bmatrix} -\cos(\sqrt{\beta\omega}\frac{l}{2}) & -\sin(\sqrt{\beta\omega}\frac{l}{2}) & e^{\sqrt{\beta\omega}\frac{l}{2}} & e^{-\sqrt{\beta\omega}\frac{l}{2}} \\ -\sqrt{\beta\omega} & -\gamma & -\sqrt{\beta\omega}-\gamma & \sqrt{\beta\omega}+\gamma \\ \cos(\sqrt{\beta\omega}\frac{l}{2}) & \sin(\sqrt{\beta\omega}\frac{l}{2}) & e^{\sqrt{\beta\omega}\frac{l}{2}} & e^{-\sqrt{\beta\omega}\frac{l}{2}} \\ 0 & -1 & 1 & -1 \end{bmatrix} \begin{bmatrix} A_c \\ A_s \\ A_p \\ A_n \end{bmatrix} = \begin{bmatrix} 0 \\ 0 \\ 0 \\ 0 \end{bmatrix} \tag{2.9}$$

Finally, the frequency of the system can be obtained by solving ω that makes the determinant of the matrix zero.

Figure 2.5 shows the relation between analytical frequency and the reduced stiffness of the numerical model, which is obtained from equation 2.4, the relation between crack thickness and the reduced stiffness, and the analytical frequency as a function of the damage thickness. In the third figure, it is observable that the local stiffness reduction reduces the frequency with small amount, which makes the damage even harder to detect.

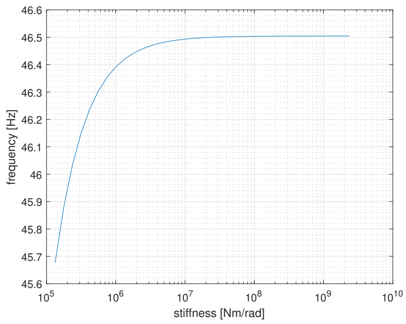

(a) Frequency vs stiffness

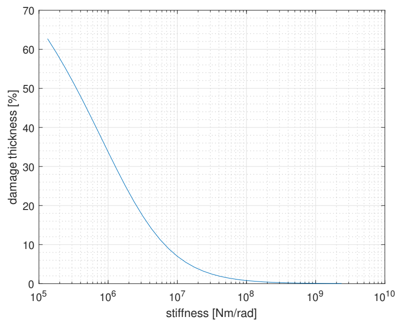

(b) Damage thickness vs stiffness

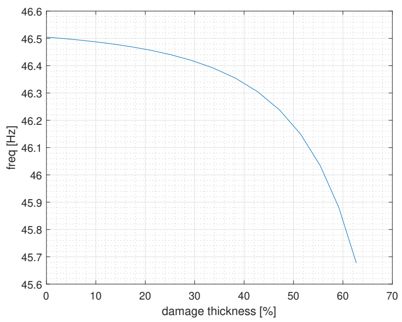

(c) Frequency vs damage thickness

Figure 2.5: Relation of damage thickness, reduced stiffness, and analytical frequency

Eigenvalues analysis is performed in the multibody model in order to find the first natural frequency of the multibody model, using MBDyn. Two types of model are used: 8 elements beam and 16 elements beam. For both of them, the natural frequency is computed at several damage thickness value, which are 0.1%, 1%, 3%, 5%, 7%, and 10% damage. The result is compared with the first natural frequency, obtained by solving the analytical equation by solving ω that makes the determinant of the matrix zero, in equation 2.14.

Figure 2.6 shows the difference in first natural frequency of the 8 elements beam, 16 elements beam, and the result of analytical solution. As expected, all of them shows degradation of frequency due to increase of damage. The frequency obtained by using infinite stiffness in the analytical solution is 46.5046 Hz, which is the same result obtained from the analytical frequency of simply supported beam, shown in equation 2.10.

$$\omega = \sqrt{\frac{EJ_y}{m}}(\frac{\pi i}{l})^2 \tag{2.10}$$

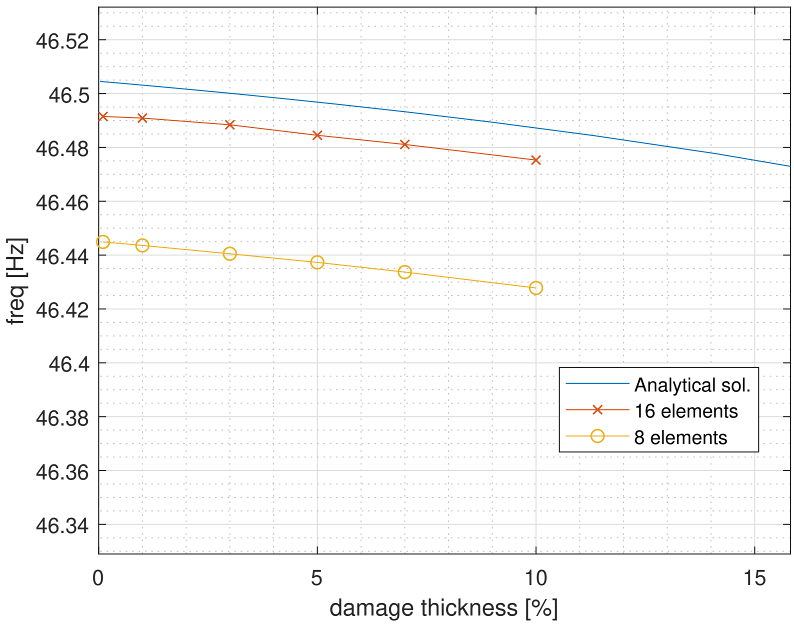

Figure 2.6: Frequency vs damage thickness

It is visible in figure 2.6 that by increasing the number of element used, the natural frequency is closer to the analytical solution frequency. In terms of first natural frequency, the 8-elements beam model has error around 0.13%, while the 16-elements beam has error around 0.03%. In conclusion, the 16-elements beam multibody model is enough to represent the problem.

The decrease in natural frequency is small when the percentage of damage is small. This makes early damage detection rather difficult, if only the frequency is used. Furthermore, frequency domain approaches based on modal shape analysis require more measurement points, which increase cost and complexity of the problem (Serafini et al., 2019).

From figure 2.6, it is evident that the lower the damage thickness, the lower is the change of natural frequency of the structure. It is assumed that damage thickness less than 1% does not change the frequency. Furthermore, small damage thickness can be present during the manufacturing process of the structure. Therefore, the whole beam model, 0.001%, and 0.1% damaged model will be used as undamaged model for the machine learning algorithm.

2.3.2 *Stiffness addition in simply supported beam*

Corrosion damage in the left support is modeled as an undesired stiffness addition. Figure 2.7 shows the picture of the problem.

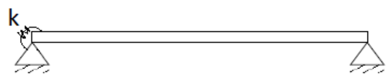

Figure 2.7: Added stiffness in simply supported beam

The principle of virtual work for the problem is written as

$$\int_0^l \delta w'' EJw'' dx + \int_0^l \delta w m\ddot{w} dx + \delta w'_{(0)} k w'_{(0)} = 0 \tag{2.11}$$

where w is the vertical displacement of the beam, E is the Young's modulus, J is the bending inertia, m is the mass per unit length of the beam, and k is the stiffness. Four boundary conditions and one main equation are obtained after integrating by part equation 2.11.

$$EJw'''' + m\ddot{w} = 0 \tag{2.12}$$

Boundary conditions:

$$\begin{cases} w_{(0)} = 0 \\ w_{(l)} = 0 \\ w''_{(l)} = 0 \\ -EJw''_{(0)} + kw'_{(0)} = 0 \end{cases}$$

Assuming solution of $w_{(x,t)} = a_{(x)}b_{(t)}$ and substituting it to equation 2.12, the following equation is obtained.

$$a(x) = A_c\cos(\sqrt{\beta\omega}x) + A_s\sin(\sqrt{\beta\omega}x) + A_p e^{\sqrt{\beta\omega}x} + A_n e^{-\sqrt{\beta\omega}x} \tag{2.13}$$

where $\beta = \sqrt{\frac{m}{EJ}}$. Using $\gamma = \frac{k}{EJ}$, equation 2.13 is substituted to the boundary conditions to obtain a system of equation.

$$\begin{bmatrix} 1 & 0 & 1 & 1 \\ \cos(\sqrt{\beta\omega}l) & \sin(\sqrt{\beta\omega}) & e^{\sqrt{\beta\omega}l} & e^{-\sqrt{\beta\omega}l} \\ -\cos(\sqrt{\beta\omega}l) & -\sin(\sqrt{\beta\omega}) & e^{\sqrt{\beta\omega}l} & e^{-\sqrt{\beta\omega}l} \\ -\sqrt{\beta\omega} & -\gamma & \sqrt{\beta\omega}-\gamma & \sqrt{\beta\omega}+\gamma \end{bmatrix} \begin{bmatrix} A_c \\ A_s \\ A_p \\ A_n \end{bmatrix} = \begin{bmatrix} 0 \\ 0 \\ 0 \\ 0 \end{bmatrix} \tag{2.14}$$

Finally, the frequency of the system can be obtained by solving ω that makes the determinant of the matrix zero. The result from MBDyn's eigenanalysis is compared to the analytical natural frequency in figure 2.8.

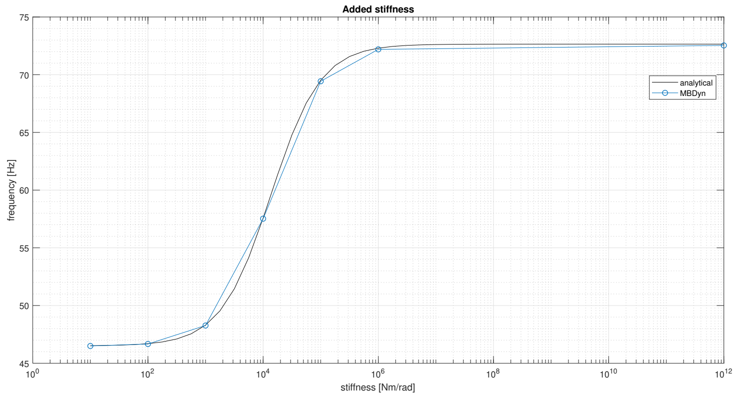

Figure 2.8: Frequency vs added stiffness

In figure 2.8, it is observable that the structure behaves similar to a simply supported beam in the range of small stiffness addition and asymptotically goes to the natural frequency of clampled - simply supported beam when the stiffness is increased.

2.4 MULTIVARIATE AUTOREGRESSIVE MODEL

Multivariate Autoregressive model is a linear multivariate time series model which characterises interregional dependencies within data, in terms of the historical influence of each variables (Penny and Harrison, 2006). It is used to find the parameter that represents the model from the time-series data of displacement, using two variables, which are the displacement of the first and second nodes.

An Autoregressive model (AR) is a simple and effective approach for time series characterisation (Penny and Harrison, 2006). Univariate time series data contains information about the process that constructed it. In Autoregressive model, the order of the process can be determined by modelling the current value of the variable as a weighted sum of its previous value.

In Multivariate Autoregressive model, the previous approach is extended to multiple time series by expressing the vector of the current values of the variables as a linear sum of the previous value. A Multivariate Autoregressive model of order m forecasts the next value of the d variables time series y_n as a linear combination of the m previous vector, added with a Gaussian zero mean noise $e_n = [e_n(1), e_n(2), ..., e_n(d)]$.

$$y_n = \sum_{i=1}^{m} y_{n-1} A(i) + e_n \tag{2.15}$$

where $y_n = [y_n(1), y_n(2), ..., y_n(d)]$ is the nth sample of a d-dimensional time series and $A(i)$ is a d-by-d matrix of coefficients of the model.

The model in equation 2.15 can be written in standard form of multivariate linear regression model.

$$y_n = x_n W + e_n \tag{2.16}$$

where $x_n = [y_{n-1}, y_{n-2}, ..., y_{n-m}]$ are the m previous multivariate time series samples and W is a (m x d)-by-d matrix of the Multivariate Autoregressive model coefficients. The number of independent coefficients are k= m x d x d coefficients.

For N samples in the time series, equation 2.17 can be written.

$$Y = XW + E \tag{2.17}$$

where Y is an (N-m)-by-d matrix, X is an (N-m)-by-(m x d) matrix, and E is an (N-m)-by-d matrix. The number of rows are N-m, because at time point before m, the model does not have sufficient samples to predict forward.

Maximum likelihood estimation is used in order to find the Multivariate Autoregressive model coefficients. The Maximum Likelihood solution for the coefficients is obtained by solving a least-square problem.

$$\hat{W} = (X^T X)^{-1} X^T Y \tag{2.18}$$

where $\hat{W}$ is a (m x d)-by-d matrix of the estimated Multivariable Autoregressive coefficients. The parameters used for the machine learning algorithm are the coefficients of matrix $\hat{W}$.

2.5 MAHALANOBIS SQUARED DISTANCE

The process in novelty detection can be performed by assuming a known shape of the probability distribution of the features that define the normal condition. In this method, by using Gaussian distribution assumption, the data can be represented by its first two statistical moments, which are the mean and variance (or covariance for multidimensional feature vectors). The drawback is that the assumption of Gaussian distribution in the data is not always valid.

In statistics, the problem of novelty detection is in the context of outlier analysis. The main idea is to compute an index for the data and then compare it to a given threshold. If the index exceeds the given threshold, the data of the index is labeled as an outlier. For univariate data, the discordancy measures are based on statistics of the normal condition data.

$$z = \frac{|x_\zeta - \bar{x}|}{\Sigma_x} \tag{2.19}$$

where x_ζ is the candidate outlier that is tested, and $\bar{x}$ and Σ_x are the mean and standard deviation of the reference data sample. The measure in equation 2.19 is not restricted to a Gaussian distribution condition, but it is a scaled distance from the mean of the reference data.

Often in practice, multiple characteristics data are analyzed. A measure of distance between groups in terms of multiple characteristics is defined. The most often used measure is the Mahalanobis distance, which is proposed in 1930 (Mahalanobis, 1930) in the context of study of racial likeness (McLachlan, 1999). Since then, it has been used in statistics and data analysis of multiple measurements in many application, such as numerical taxonomy and statistical pattern recognition, from archaeology to medical diagnosis to remote sensing (McLachlan, 1999).

To check the damage index of a feature vector x_i, equation 2.20 is used.

$$DI_i = (x_i - \bar{x})^T [\Sigma]^{-1} (x_i - \bar{x}) \tag{2.20}$$

where $\bar{x}$ and $[\Sigma]$ are the mean feature vector and covariance matrix of the normal condition feature.

If a feature vector is obtained from damaged system, the damage index will have high value. While if a feature vector is coming from undamaged system, the damage index will have low value, because the equation used in 2.20 has been trained with the reference undamaged data. The result from equation 2.20 is compared to a threshold value to classify if the data comes from an undamaged or damaged model. If the damage index is higher than the threshold, then it is classified as damaged.

2.6 RESULTS

The response of the model is computed using multibody solver MB-Dyn. Displacement time-series data of the first and second nodes located at $\frac{15}{32}L$ and $\frac{3}{4}L$ are used to build the multivariable autoregressive model. Then, the coefficients of the multivariable autoregressive model are used as the features for the machine learning algorithm using Mahalanobis squared distance. To verify the result, the parameter of the damaged model is tested on the machine learning model.

The training data matrix, obtained from the whole beam model, 0.001%, and 0.1% damage are used as the reference of the healthy model. It contains 100 samples, which consist of 40 samples from the whole model, 30 samples from 0.001% damaged model, and 30 samples from 0.1% damaged model. The training phase is performed by calculating the mean feature vector and covariance matrix of the training data set.

Four different types of damaged model are used: The crack damage of 1%, 5%, and 10% of the thickness simulated with reduction of spring stiffness with both linear and nonlinear constitutive law, the beam model with the added mass in the middle of 0.01%, 0.1%, and 1% of the total weight, the beam model with 0.1% added mass in the left quarter, and the beam model with added stiffness in the left support. Table 2.2 shows the list of structural state conditions.

Table 2.2: List of structural state conditions

State	Condition	Description
1	Undamaged	Reference
2	Damaged	1% damage
3	Damaged	5% damage
4	Damaged	10% damage
5	Damaged	1% nonlinear damage
6	Damaged	5% nonlinear damage
7	Damaged	10% nonlinear damage
8	Undamaged	0.01% added mass in the middle
9	Damaged	0.1% added mass in the middle
10	Damaged	1% added mass in the middle
11	Damaged	0.1% added mass in the left quarter
12	Damaged	10 Nm/rad added stiffness
13	Damaged	100 Nm/rad added stiffness

Each samples are collected from 50 second displacement measurement of the first and second nodes. The ARX model is fitted to the displacement time-series, then the coefficients of the ARX model are stored as a feature vector. Three different order of the Multivariate Autoregressive model are used: 4,5, and 6.

The threshold line decides if a sample is classified as damaged or undamaged sample. A sample with damage index lower than the threshold is classified as undamaged, while sample with damage index higher than the threshold is classified as damaged.

Determining the threshold used is an important aspect in the classification process. Some authors proposed Monte Carlo simulation to determine the threshold (Gul and Catbas, 2009), while others set a predefined value based on the percentage cut-off value over the training data. The threshold used in this work is 95 percentile of the damage indicator of the training data set.

Figure 2.9,2.10, and 2.11 show the damage index of the reference data and the test data, obtained from multivariate Autoregressive model order 4, 5, and 6 respectively. Red-colored dots indicate data that are classified as damaged, while black-colored dots are used for data that are classified as undamaged.

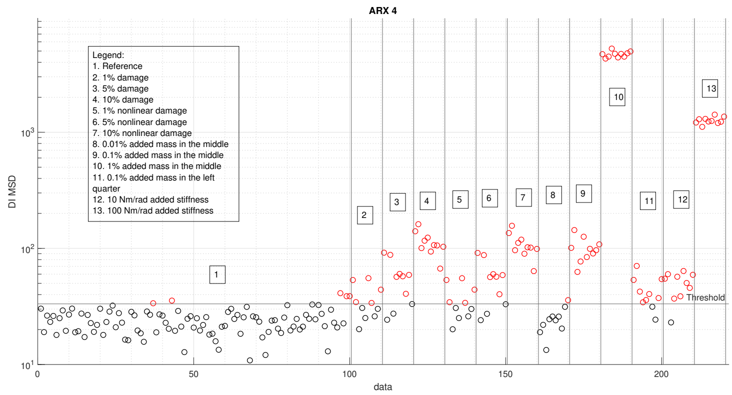

Figure 2.9: Damage indicator for ARX4 model

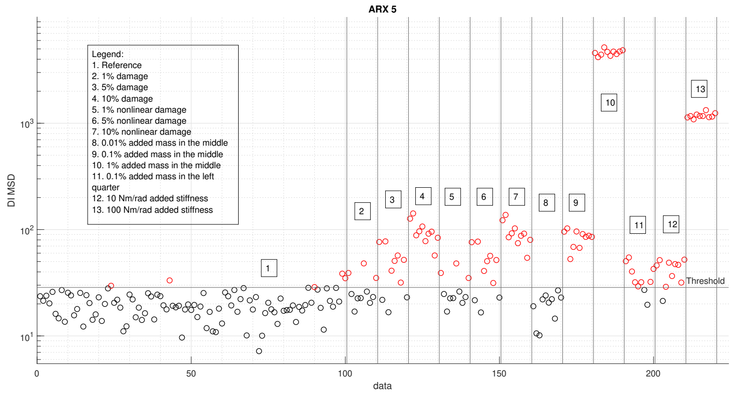

Figure 2.10: Damage indicator for ARX5 model

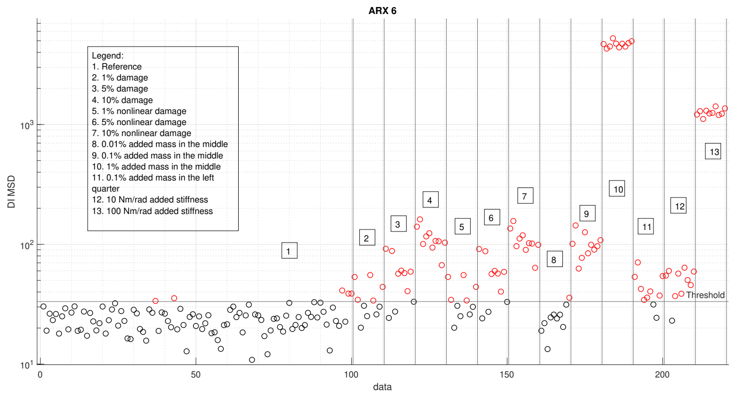

Figure 2.11: Damage indicator for ARX6 model

The same random loads are used for the nonlinear and linear crack model. The nonlinear crack model shows lower damage index compared to the linear stiffness model. In the nonlinear model, a very high stiffness is used when the crack is closing and a reduced stiffness is used when the crack is opening, while in the linear model, the constitutive law applies the reduced stiffness for both condition. In terms of response, the behaviour of the nonlinear model is closer to the reference undamaged data compared to the linear model.

The results show that the 10% damage both for linear and nonlinear, 0.1% and 1% added mass, and 100Nm/rad added stiffness model are identified correctly as damaged by all of the Multivariate Autoregressive model.

The 0.01% added mass model are classified as undamaged data by all of the Multivariate Autoregressive model, since the damage index is below the threshold. Eigenanalysis shows that the first natural frequency of the model is 46.48 Hz, which is very close to the reference model. It is safe to identify it as undamaged data, since the addition of mass is small. Moreover, variability of the structure due to manufacturing process may occurs in the structure.

The 0.1% added mass in the left quarter model display lower damage index compared to the added mass in the middle. Location of the added mass influences the result of the detection process. Added mass in the middle gives more severe damage index.

The Multivariate Autoregressive model of order 4,5, and 6 show confusion in detecting small damages of 1% and 5%. It happens due to the similar response of the system, which makes the damage detection process harder. For these sets of data, the different order model does not show significant changes in the result.

Overall, the reduced stiffness model is the hardest to be identified. It happens due to the small differences in frequency that cannot be identified by the algorithm.

To quantify the performance of the classifier, type I (false-positive damage indication) and type II (false-negative damage indication) error is calculated. Table 2.3 shows the type I and type II error for each model.

Table 2.3: Percentage of Type I and Type II errors for each algorithm

		Type I	error[%]		Type II	error[%]	
State	Description	ARX4	ARX5	ARX6	ARX4	ARX5	ARX6
1	Reference	5	4	5			
2	1% damage				50	70	50
3	5% damage				30	30	30
4	10% damage				0	0	0
5	1% nonlinear damage				50	70	50
6	5% nonlinear damage				30	30	30
7	10% nonlinear damage				0	0	0
8	0.01% added mass in the middle	10	0	10			
9	0.1% added mass in the middle				0	0	0
10	1% added mass in the middle				0	0	0
11	0.1% added mass in the left quarter				20	20	20
12	10 Nm/rad added stiffness				10	10	10
13	100 Nm/rad added stiffness				0	0	0

In this work, different factors that might influence the results such as temperature and humidity are not yet analysed. It is well known that changes in temperature generates stresses that influences the behavior of the structure in terms of frequency.

3 HELICOPTER ROTOR BLADES SHM

Nothing in life is to be feared, it is only to be understood. Now is the time to understand more, so that we may fear less.

— *Marie Curie*

3.1 INTRODUCTION

In this work, structural health monitoring algorithm is applied to helicopter rotor blades based on measurement of strain in the blades. Helicopter rotor blades are rotating flexible structure which are subjected to multiple dynamic loads. They provide lift and control of the helicopter and transmit loads to the rotor hub. They are one of the most critical structure on the helicopter, since damages might lead to loss of lift and control.

The damages in a helicopter rotor blades can be caused by numerous reason. Some of them are delamination, debonding, corrosion, or local impact from accidental foreign object. The presence of damage, combined with the extreme operating environment of high velocity and load might trigger catastrophic failure of the structure. It is important to detect and identify the damage before failure. When the indicator shows presence of damage, the blade will be removed and analysed for further inspection.

The simulation of the phenomena is performed numerically using a multibody dynamic solver MBDyn for comprehensive aeroelastic analysis of rotorcraft. The advantages of using the codes are the possibility to modify the mechanical properties of the model and simulate the damage. Localized stiffness reduction is used to simulate damage.

The damage detection algorithm uses the measurement of signals from strain sensors located on different blades. Three algorithms are presented. They are based on the differences between the strains on damaged and undamaged blades. The type of damage considered is torsional stiffness reduction.

Three machine learning algorithms for novelty detection are performed: Mahalanobis squared distance, auto-associative neural network, and singular value decomposition. The training and test data are obtained from the time-series output of MBDyn model. The time-series of torsional shear strain measurement are copied and injected with random noises to simulate in several experiments. The features used are the mean value criterion of the differences signal.

3.2 ROTOR MODEL

The rotor model used for this analysis is Bo105, developed in the field of research GARTEUR HC AG-16 RPC, which consist of collaboration between helicopter company and universities. It is a four-blade hingeless rotor, with radius of 4.9m, rotating at 44.4rad/s. It is flying on a constant forward-flight at a constant advance ratio $\mu = 0.2$, which is the ratio of the forward velocity and the rotor blade tip velocity in hovering. The blades have 0.23m offset from the hub with precone angle 2.5°. From the end of the flexbeam element to the tip, the blades are twisted linearly with value of -6.23° at the tip.

The placement of the sensors considers the value of signal to noise ratio. Maximum signal to noise ratio can be obtained by placing the sensors near the root. Based on that consideration, the strain sensors are placed at 20% of the chord at 10% of the blade span. Blade number 1 is subjected to damage modification.

3.2.1 *Damage simulation*

The damage considered in the simulation is localized reduction of torsional stiffness in the helicopter blade. Rather than introducing a beam element with reduced stiffness, two beams connected with a torsional spring are used which represent the equivalent beam.

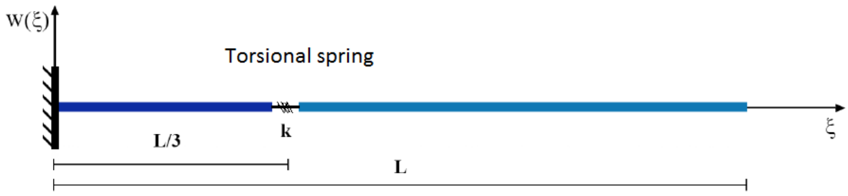

Figure 3.1: Beam with torsional spring

Figure 3.2 shows the torsional stiffness profile of the equivalent beam. G is the shear modulus, J is the torsional moment of inertia, L_d is the longitudinal length of damage, and ξ is the longitudinal axis of the beam.

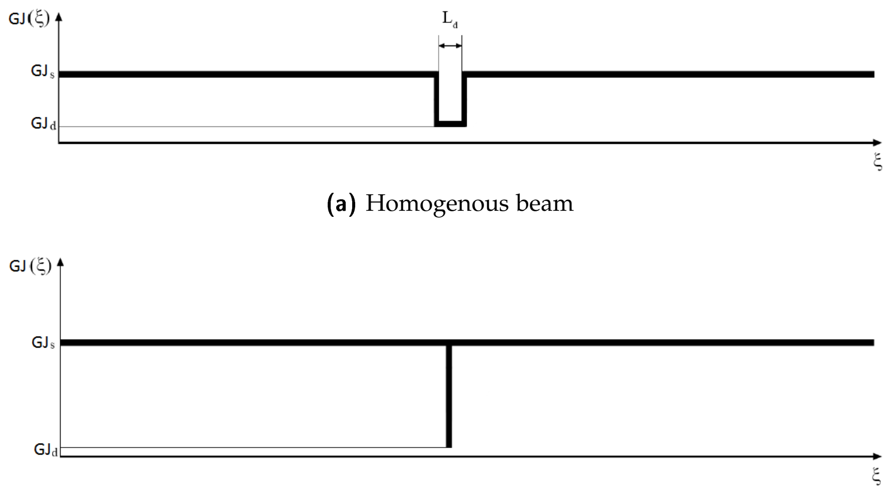

(a) Homogenous beam

(b) Equivalent beam

Figure 3.2: Torsional stiffness profile of the equivalent beam

To determine the spring constant, the equivalent torsional angle is taken into account.

$$\int_{r-\frac{L_d}{2}}^{r+\frac{L_d}{2}} \frac{M_t}{GJ_d} dx = \int_{r^-}^{r-\frac{L_d}{2}} \frac{M_t}{GJ_u} dx + \Delta\phi + \int_{r^+}^{r+\frac{L_d}{2}} \frac{M_t}{GJ_u} dx \tag{3.1}$$

where ϕ is the torsional angle, M_t is the torsional moment, GJ_u is the undamaged stiffness, GJ_d is the damaged stiffness.

Assuming small L_d with no discontinuity of torsional moment, the spring constant value of the torsional spring is obtained.

$$K = \frac{\frac{1}{L_d}}{\frac{1}{GJ_d} - \frac{1}{GJ_u}} \tag{3.2}$$

Figure 3.3 shows the reduction of the equivalent spring stiffness as a function of the stiffness reduction, obtained from equation 3.2

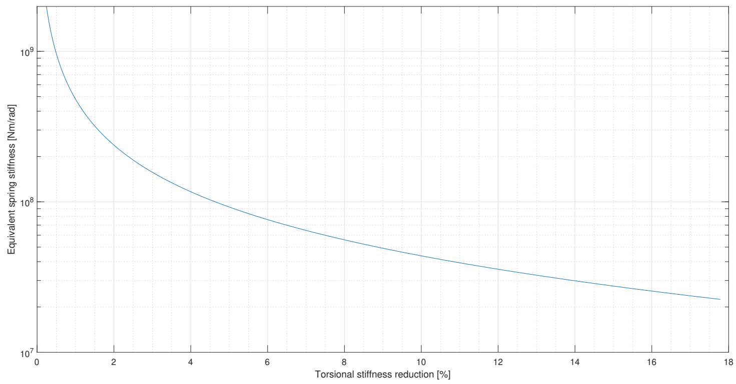

Figure 3.3: Equivalent spring stiffness

3.2.2 *Strain displacement relation*

Geometrically exact nonlinear beam finite elements (Ghiringhelli, Masarati, and Mantegazza, 2000) is used in the rotor blades. The strains are evaluated from the beam displacements using nonlinear relations, proposed by Hodges and Dowell, 1974. The strain tensor **E** is reported in equation 3.3.

$$\mathbf{E} = \begin{bmatrix} \epsilon_{\xi\xi} & \epsilon_{\xi\eta} & \epsilon_{\xi\zeta} \\ \epsilon_{\xi\eta} & -\nu\epsilon_{\xi\xi} & 0 \\ \epsilon_{\xi\zeta} & 0 & -\nu\epsilon_{\xi\xi} \end{bmatrix} \tag{3.3}$$

where ξ axis is tangent to the elastic axis, η and ζ are cross-section principal axes. The strain-displacement are

$$\begin{aligned} \epsilon_{\xi\xi} &= u' + \frac{1}{2}(v'^2 + w'^2) - \lambda\phi'' + (\eta^2 + \zeta^2)(\theta'\phi' + \frac{\phi'^2}{2}) \\ &-v''(\eta\cos(\theta+\phi) - \eta\sin(\theta+\phi)) - w''(\eta\sin(\theta+\phi) + \eta\cos(\theta+\phi)) \end{aligned} \tag{3.4}$$

$$\epsilon_{\xi\eta} = -\frac{1}{2}(\zeta + \frac{\partial\lambda}{\partial\eta})\phi' \tag{3.5}$$

$$\epsilon_{\xi\zeta} = \frac{1}{2}(\eta - \frac{\partial\lambda}{\partial\zeta})\phi' \tag{3.6}$$

where u, v, and w are axial, lag, and flap displacements of the elastic axis, θ is the build-in twist angle, ϕ is the blade cross-section elastic torsion, and λ is the section warping function. The warping function λ will be neglected for the sake of simplicity. However, the effect of the warping function can be included if necessary by following some numerical finite element approach or experimental activity from a known-displacement calibration test (Serafini et al., 2018).

For torsional type of problem, the shear strain signal is the most relevant measurement. Only the shear strain signal in equation 3.5 is used as an input to the structural health monitoring algorithm.

The first derivative of the torsional angle ϕ' is approximated using central difference. It is expressed as a function of the torsional angle of the nodes before and after the measured nodes, divided by the longitudinal distance.

$$\phi_i' = \frac{\phi_{i+1} - \phi_{i-1}}{x_{i+1} - x_{i-1}} \tag{3.7}$$

where ϕ is the torsional angle and x is the longitudinal location of the nodes.

3.3 METHODOLOGY

The algorithms are first proposed and developed by Serafini et al., 2019. They use the difference between strain measurements from the sensors on the i-th and j-th blades. Three algorithms are presented: Autocorrelation criterion, Power Spectral Density criterion, and mean value criterion.

Time signals from different sensors on different blades are used to identify the behaviour of the blades. Considering a four-bladed helicopter in stationary forward flight with identical blades, the measured strain signals are periodic with phase shift $\frac{2\pi}{4}$. In a four-bladed rotor where there are differences in terms of stiffness or mass in one of the blade, the measured signals will have different characteristic.

First, the signal from each strain measurement are collected. Then, the difference signal is obtained by calculating the difference between each 4 signals, which results in 6 signals (1-2, 1-3, 1-4, 2-3, 2-4, and 3-4). All the difference signals $\Delta s_{ij}(t)$ are normalized with the reference signal $\Delta s_{ij}^{ref}(t)$, which are obtained from a model with no damage in all blades.

$$\Delta\Delta s_{ij}(t) = \Delta s_{ij}(t) - \Delta s_{ij}^{ref}(t) \tag{3.8}$$

The characterization of the reference delta signal Δs_{ij}^{ref} requires a calibration process of measuring the Δs_{ij} after the track and balance procedure, in different flight conditions. Several parameters like flight level and weight might not be able to be considered during the calibration process, therefore the $\Delta\Delta s_{ij}$ signal may not be exactly zero for pairs of undamaged blades. However, if damage is present in the blade, a significant increase in the $\Delta\Delta s_{ij}$ signal is expected.

3.3.1 *Analysis in time domain*

The resulting signals $\Delta\Delta s_{ij}(t)$ are analysed using autocorrelation. The normalized autocorrelation signal between undamaged and undamaged blade contains only noise and transient response effect. When the $\Delta\Delta s_{ij}(t)$ signal involves a damaged blade, the autocorrelation signal between damaged and undamaged blade will be periodic with higher magnitude.

$$c_{ij}(\tau) = \frac{1}{T}\int_{-\frac{T}{2}}^{\frac{T}{2}} \Delta\Delta s_{ij}(t)\Delta\Delta s_{ij}(t+\tau)d\tau \tag{3.9}$$

3.3.2 *Analysis in frequency domain*

In frequency domain, one can identify in which frequency the differences happen. Without the damage, the aeroelastic response of the differences signal are similar. The power spectral density of the differences signal is characterized by some peaks at the multiple of the rotational velocity of the rotor Ω.

Welch algorithm is used to compute the power spectral density. The parameters used in the algorithm are displayed in table 3.1.

Table 3.1: Pwelch parameters

Samples	Sampling frequency [Hz]	Windows	overlap[%]
16000	160	10 - Blackman - Harris	50

3.4 MACHINE LEARNING ALGORITHMS

The mean value criterion described of the differences signal is used as the feature of the machine learning model. In order to construct a data set of undamaged and damaged model, the time-series of shear strain measurement is copied 100 times and each copy is corrupted with Gaussian noise vector with deviation standard $10^{-}8$. The reference data set contains the undamaged model, while the test data set is the simulation of 5% torsional stiffness reduction in blade 1, 10% torsional stiffness reduction in blade 2, and multiple damage of 5% and 1% stiffness reduction in blade 1 and 2.

Three machine learning algorithms for novelty detection are performed: Mahalanobis squared distance, auto-associative neural network, and singular value decomposition. The discussion related to Mahalanobis squared distance is already presented in chapter 2.

3.4.1 *Auto-associative Neural Network*

The artificial neurons were invented by McCulloch and Pitts, 1943. Here, the neurons receive a set of inputs and produce a single output. In McCulloch-Pitts (MCP) model, both the inputs and outputs are only binary. The input values x_i are multiplied by a weighted factor w_i before they go to the body of the neuron. An activation signal z is obtained by summing the weighted inputs.

$$z = \sum_{i=1}^{n} w_i x_i \tag{3.10}$$

The signal z is then passed through an activation function f_β, which maps the signal z to the output y. Figure 3.4 depicts the MCP neuron structure which consists of two blocks: summation and activation.

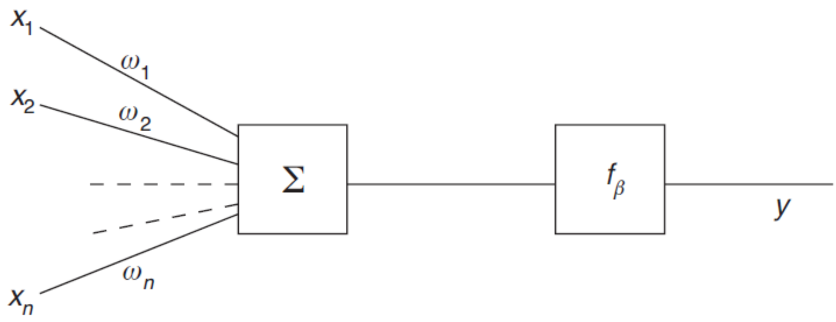

Figure 3.4: McCulloch-Pitts neuron (Farrar and Worden, 2013)

In the MCP model, the activation function f_β is a hard threshold function. The neuron fires an output 1 if the weighted sum z passed some predefined threshold β, if

$$z > \beta \tag{3.11}$$

and it does not fire an output (0), if

$$z \leqslant \beta \tag{3.12}$$

The MCP alone has limited computational proficiency. Rosenblatt, 1957 proposed a model of artificial neural networks called the perceptron which contains three-layered network. The first processing layer is the associative layer, while the second layer gives output signal of the model, displayed in figure 3.5. The name perceptron was given due to its application in pattern recognition within an image.

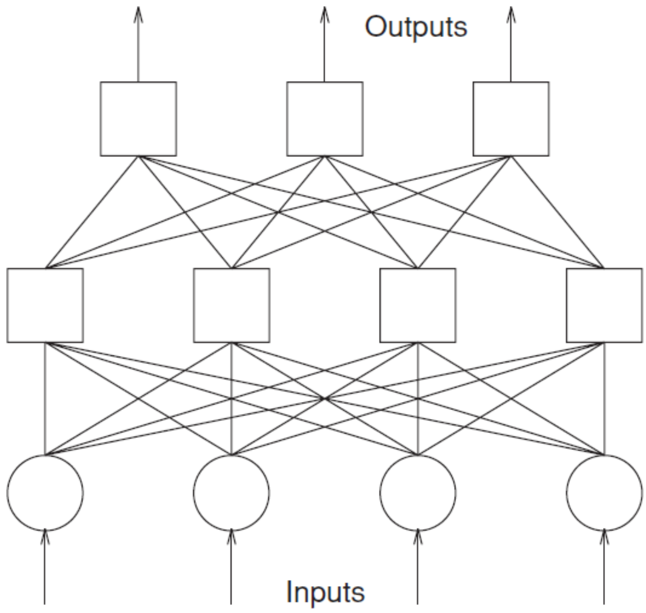

Figure 3.5: Rosenblatt's perceptron (Farrar and Worden, 2013)

A learning algorithm for multilayer structures is not easily defined, due to the use of hard threshold as an activation function in the individual neurons. Therefore, solutions of replacing the hard threshold function with a continuous function such as the sigmoid function in 3.13 or hyperbolic tangent function in 3.14 are used.

$$y = \frac{1}{1 + e^{-z}} \tag{3.13}$$

$$y = \tanh(z) \tag{3.14}$$

The backpropagation rule which is a gradient descent algorithm for optimisation is used as the learning algorithm. By using a continuous activation function in the neurons, the problem is solved by using the chain rule of partial differentiation.

The first step of training a network is to estimate the correct values of the weight w_{ij}. A set of known network inputs and outputs are used to establish the model. For each training step, a set of input is mapped through the model, resulting in outputs that can be compared with the desired outputs. In backpropagation algorithm, the error which is the difference between desired outputs $y_i(t)$ and mapped outputs $\hat{y_i(t)}$ are passed backwards to adjust the weight in order to reduce the error. For each training set, the network error J is

$$J(t) = \frac{1}{2}\sum_{i=1}^{n^{(l)}}(y_i(t) - \hat{y_i(t)})^2 \tag{3.15}$$

where $n^{(l)}$ is the number of output layer nodes and t is an integer labels the order of the training sets. J is a function of the network weight parameter. After presentation of a training set, the descent algorithm adjust the parameters according to

$$\Delta w_i = -\eta \frac{\partial J}{\partial w_i} = -\eta \nabla_i J \tag{3.16}$$

where ∇_i is the gradient operator and η is the learning coefficient. If η is too small, convergence will be slow, while if η is too large, the parameters may diverge.

An auto-associative neural network is a feedforward neural network that maps the input to itself through a hidden bottleneck layer (Farrar and Worden, 2000). By implementing a bottleneck layer, which is a layer with fewer nodes than the input layer, the algorithm will study the dependency of each input features.

The network is trained using features from the undamaged data. To calculate the damage index of a new feature vector, equation 3.17 is used.

$$DI = ||\vec{y} - \hat{\vec{y}}|| \tag{3.17}$$

where $\vec{y}$ is the input feature vector and $\hat{\vec{y}}$ is the output feature vector of the neural network model. If the feature vector is coming from an undamaged condition, the damage index will be close to zero, while if a feature vector is coming from a damaged condition, the damage index will be high.

3.4.2 *Singular value decomposition*

Singular value decomposition for damage detection works by factorization of a rectangular matrix M. The implementation of singular value decomposition for data normalization to detect the presence of damage is first proposed by Ruotolo and Surace, 1999.

$$[M] = [U][\Lambda][V]^H \tag{3.18}$$

where [U] and [V] are two orthogonal matrices and $[\Lambda]$ is a diagonal matrix that contains the singular values of matrix [M].

First, the singular value of the training matrix [X] is computed and stored in a vector s_M. Second, a new matrix $[M']$ is formed by augmenting [X] with the feature vector y_i whose damage index is going to be calculated.

$$[M'] = [[X], y_i] \tag{3.19}$$

Third, the singular value of matrix [M′] is calculated and kept in a new vector $s_{M'}$. Finally, the damage index is measured as the Eucledian distance between the singular value vector of the training undamaged data and the singular value vector of the concatenated matrix in equation 3.19.

$$DI = \|s_M - s_{M'}\| \tag{3.20}$$

The process are repeated for all feature vector in the test data set.

3.5 RESULTS

3.5.1 *Autocorrelation, Power Spectral Density, and mean-value criterion*

Four cases of damage are simulated. The first is 10% torsional stiffness reduction in blade 1. The second is 5% torsional stiffness reduction in blade 1. The third is 5% torsional stiffness reduction in blade 1 with maneuvered flight. Two 1 - cos collective doublet excitations are imposed to the rotor in steady flight. They are separated by 4s and characterized by $\frac{\pi}{2}$ and $\frac{\pi}{4}$ rad/s with 0.5° and 0.6° amplitude respectively. The last case is 5% torsional stiffness reduction in blade 1 and 1% torsional stiffness reduction in blade 2. The localized damage is located at 33% of the main rotor radius in all of the cases.

Figure 3.6 shows autocorrelation signals over 100 revolutions in presence of 5% and 10% torsional stiffness reduction. The signals which involves blade 1 have a triangular shape. The higher the amount of damage, the higher is the peak in the autocorrelation signals. It is visible that the autocorrelation signals are symmetric at zero. The signals from 10% torsional stiffness reduction case show higher oscillation than the signals from 5% torsional stiffness reduction. The autocorrelation signals from pair of undamaged blades display low amplitude compared to the signal from damaged - undamaged blade.

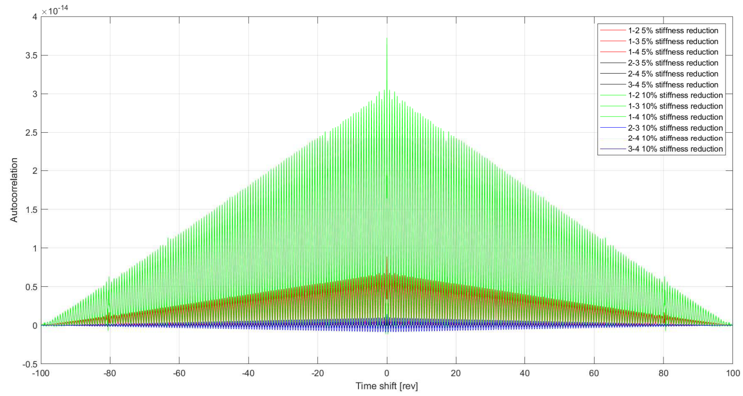

Figure 3.6: Autocorrelation signals of 10% and 5% stiffness reduction cases

Figure 3.7 shows the power spectral density of the $\Delta\Delta s_{ij}(t)$ signals from the first and second cases, which are 10% and 5% torsional stiffness reduction in blade 1. Large discrepancy is obtained at zero frequency and the multiplication of the rotational speed of the rotor from the signals that involve damaged blade. The peaks are higher for the 10% torsional stiffness reduction case, compared to 5% case.

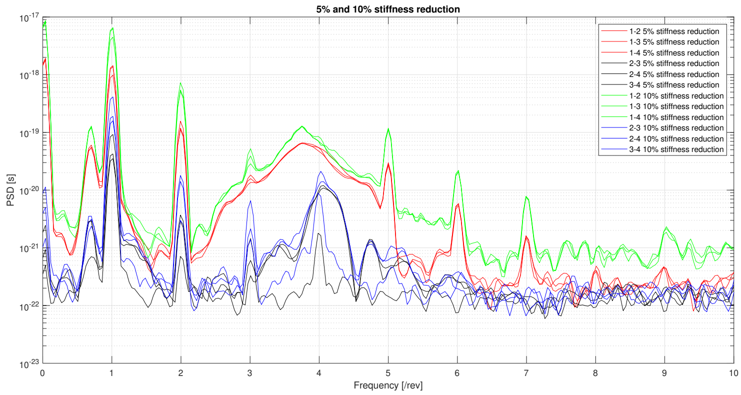

Figure 3.7: Power spectral density of 10% and 5% stiffness reduction cases

Figure 3.8 shows the autocorrelation of the $\Delta\Delta s_{ij}(t)$ signals with 5% torsional stiffness reduction in blade 1 on maneuvered flight. The beats which appear are caused by the disturbance of collective excitation. The amplitude of the damaged-undamaged signals are much larger compared to the autocorrelation of signals between undamaged-undamaged blade.

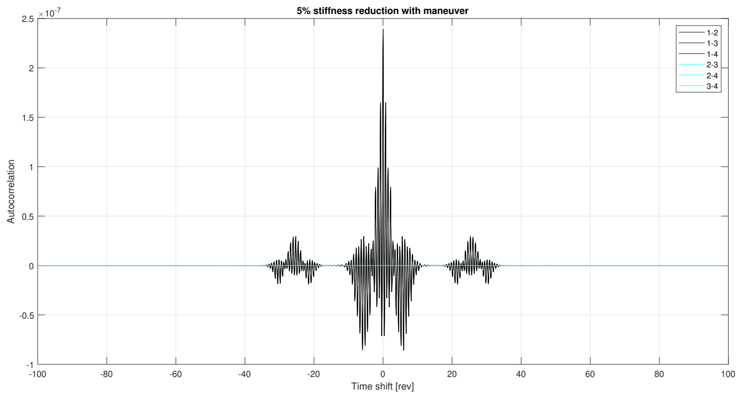

Figure 3.8: Autocorrelation signals of 5% stiffness reduction with maneuver

Figure 3.9 shows the power spectral density of the $\Delta\Delta s_{ij}(t)$ signals in presence of 5% torsional stiffness reduction in blade 1 and maneuver. The effect of excitation makes the PSD less sharp. Compared to the PSD of the signals from pair of undamaged blades, the PSD of signals from damaged-undamaged blades show higher magnitude. This means that the algorithm can identify the anomaly even in presence of maneuver.

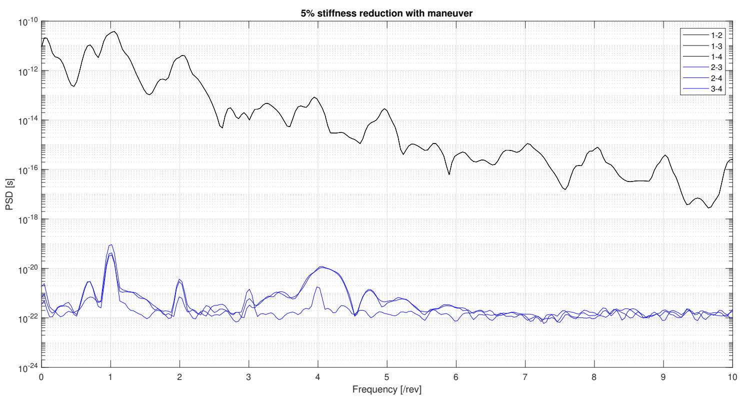

Figure 3.9: Power spectral density of 5% stiffness reduction with maneuver

Figure 3.10 shows the autocorrelation of the differences signals where the damage of 5% and 1% torsional stiffness reduction occur on the first and second blade, respectively. The autocorrelation of signals from blade 1 with blade 3 and 4 show higher oscillation, compared to the other. It is expected because blade 1 has the largest amount of damage. The autocorrelation of signals from blade 2 with blade 3 and 4 show larger oscillation compared to undamaged-undamaged blade (3 and 4), however it is smaller in terms of magnitude compared to the signals paired with blade 1.

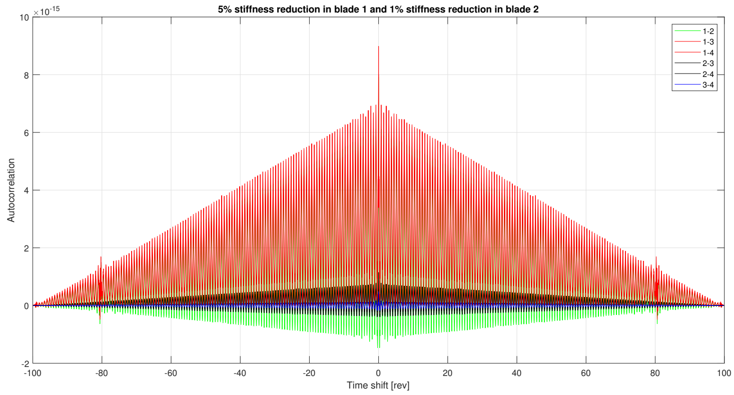

Figure 3.10: Autocorrelation of the signals with 5% stiffness reduction in blade 1 and 1% stiffness reduction in blade 2

Figure 3.11 shows the power spectral density of the $\Delta\Delta s_{ij}(t)$ signals with 5% torsional stiffness reduction in blade 1 and 1% stiffness reduction in blade 2. The PSD coming from the damaged blades gives higher value compared to the one from undamaged-undamaged blades. The PSD of the signals that are paired with blade 1 has higher magnitude compared to the PSD of the signal that are paired with blade 2.

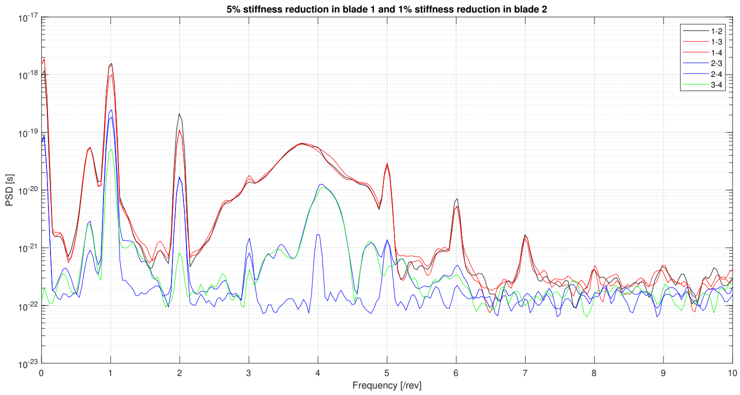

Figure 3.11: PSD of the signals with 5% stiffness reduction in blade 1 and 1% stiffness reduction in blade 2

Figure 3.12 shows the mean of the $\Delta\Delta s_{ij}(t)$ signals in all of the damage cases. The presence of damage is clearly visible in all the bars involving the damaged blade, which is blade 1. Higher value of mean is obtained from the case of 10% torsional stiffness reduction, compared to the case of 5% torsional stiffness reduction. If the signal does not involve a damaged blade, the mean value of the $\Delta\Delta s_{ij}(t)$ signal shows magnitude smaller than damaged blade. The effect of maneuver increases the mean value of the signals that involve damaged blade, however the signals from undamaged-undamaged blades remain low. In the last damage case, where blade 1 has 5% torsional stiffness reduction and blade 2 has 1% reduction, an increase in the mean value is obtained from the signals which involve blade 2. This is expected due to the presence of damage introduced in blade 2.

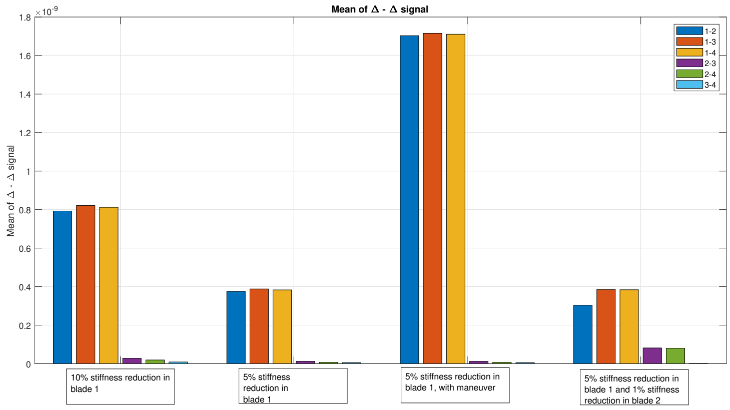

Figure 3.12: Mean of $\Delta\Delta s_{ij}(t)$ signals

The different methods displayed the ability to detect anomaly in the blade. In order to have an accurate prediction of the system, a baseline signal in different flight condition is needed. All the methods work in presence of maneuver and in case off multiple damages in different blade.

3.5.2 *Machine learning algorithms*

The data set of undamaged and damaged model, the time-series of shear strain measurement is copied 100 times and each copy is corrupted with Gaussian noise vector with deviation standard $10^{-}8$. The reference data set contains the undamaged model, while the test data set is the simulation of 5% torsional stiffness reduction in blade 1, 10% torsional stiffness reduction in blade 2, and multiple damage of 5% and 1% stiffness reduction in blade 1 and 2. Table 3.2 shows the structural state conditions.

Table 3.2: List of structural state conditions

State	Condition	Description
1	Undamaged	Reference
2	Damaged	5% stiffness reduction in blade 1
3	Damaged	10% stiffness reduction in blade 1
4	Damaged	5% and 1% stiffness reduction in blade 1 and 2

Figure 3.13 shows the autocorrelation of the $\Delta\Delta s_{ij}(t)$ when noise is present in the measurement of torsional shear strain. The effect of noise is making the autocorrelation to be less clear.

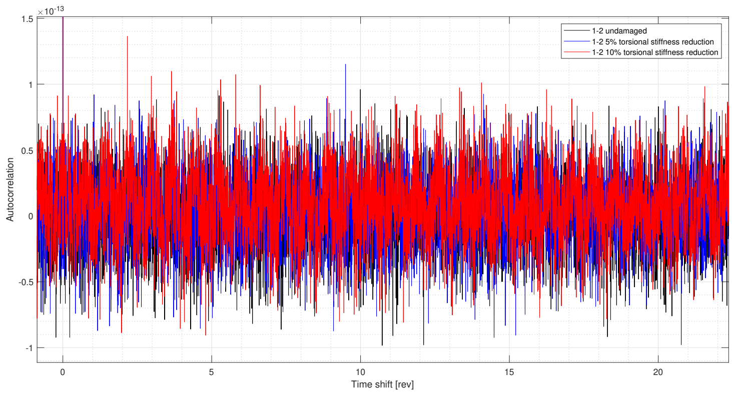

Figure 3.13: Autocorrelation of $\Delta\Delta s_{ij}(t)$ signals, corrupted with noise

Figure 3.14 shows the power spectral density of the $\Delta\Delta s_{ij}(t)$ when noise is present in the measurement of torsional shear strain. The simulation from 10% stiffness reduction case has the highest peak at 1/rev frequency.

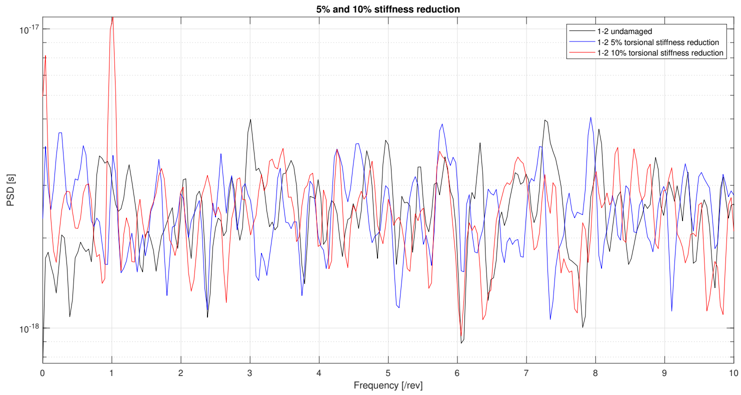

Figure 3.14: PSD of $\Delta\Delta s_{ij}(t)$ signals, corrupted with noise

The mean value criterion is selected as the feature for the machine learning algorithm. It is a six-dimension vector which consists of differences signal of blade 1-2, 1-3, 1-4, 2-3, 2-4, and 3-4.

The Mahalanobis squared distance algorithm is the simplest of the three in terms of computational efforts, since it only needs to learn the reference data by computing the mean and the covariance matrix. Auto-associative neural network algorithm has advantages in terms of discovering nonlinear relations of the features (Figueiredo et al., 2010).

Figure 3.15,3.16, and 3.17 show the damage detection result using the algorithm of Mahalanobis squared distance, auto-associative neural network, and singular value decomposition, respectively. An auto-associative neural network with 5 hidden nodes is used, since the input and the output layer have 6 nodes of neuron. The threshold used in all of them is 95% percentile of the damage index of the reference undamaged data.

The classification process works by comparing the damage index to the threshold value. The red-colored dots are instances that are identified as damaged, since they are above the threshold. The black-colored dots are identified as undamaged, because they are below the threshold.

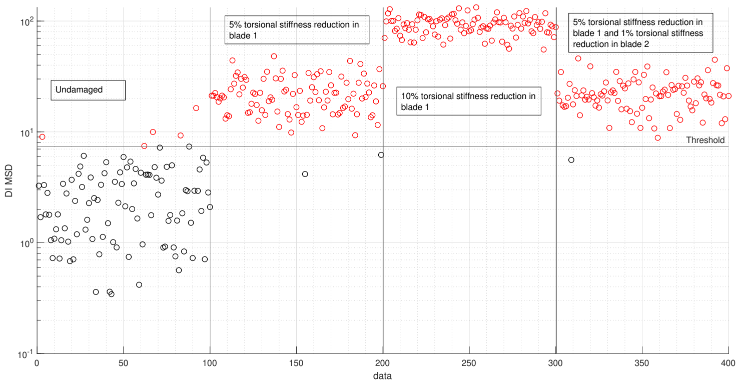

Figure 3.15: Damage index using Mahalanobis squared distance

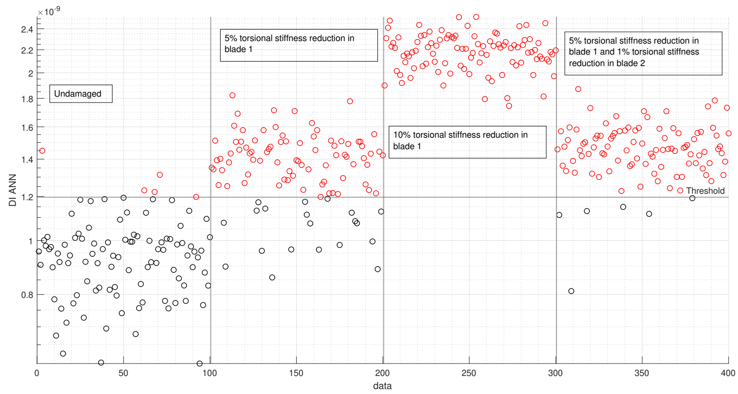

Figure 3.16: Damage index using auto-associative neural network

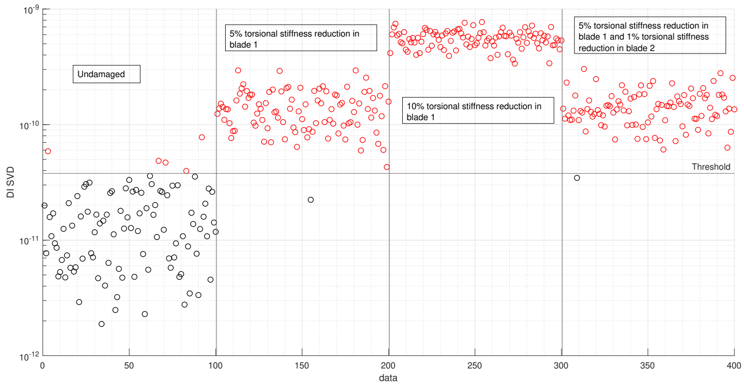

Figure 3.17: Damage index using Singular Value Decomposition

The overall accuracy of the algorithms are 98%, 92.25% ,and 98.25%. The 5% torsional stiffness reduction in blade 1 case has lower damage index than the case of 10% reduction, which is expected. Compared to the first case, the case of multiple damage does not show significant increase in damage index.

The machine learning algorithms have been tested with satisfying result. They can separate the data of damaged from undamaged cases. In terms of overall performance, the singular value decomposition algorithm has the highest accuracy, followed by Mahalanobis squared distance and auto-associative neural network.

It should be noted that the algorithms performed in this work are only limited to the range of operation presented in the simulation. It cannot guarantee a reasonable result if it is applied for different operational or environmental condition such as different flight condition.

4 CONCLUSIONS AND FUTURE WORK

4.1 simply supported beam

Damage detection is performed on two different problems: simply supported beam and helicopter rotor blades. The simulations are performed through the multibody dynamics solver MBDyn.

In the simply supported beam, multivariable autoregressive model is used on the displacement measurement. Mahalanobis squared distance is used as the machine learning algorithm to identify outliers in the data sets.

Several types of damages are presented: localized bending stiffness reduction, added mass, and added stiffness. The methods are able to identify the damage.

Future works might include a system that can predict the type, location, and severity of the damage. Supervised learning algorithm can be used in order to build such model.

4.2 helicopter rotor blades

Structural health monitoring on helicopter blades has been performed using the autocorrelation of the difference strain signals among rotor blades. The helicopter is flying in forward flight with a constant velocity. The damage is simulated as a localized torsional stiffness reduction in one of the blade.

Three algorithm which use the differences signal of strain are presented: autocorrelation criteria, power spectral density criteria, and mean value criteria. All of them are able to identify the presence of damage in the simulated systems.

The three machine learning algorithms, which are Mahalanobis squared distance, auto-associative neural network, and singular value decomposition are tested on the simulated data. The mean value criteria is used as the feature for the machine learning algorithms. They are able to identify damages that are presented in the simulation.

Future works might include application for different flight conditions and maneuvers, placement of sensors, and type of damage identification. A collection of baseline data is also needed for various steady flight conditions.

Cronkhite, J D (1993). “Practical application of health and usage monitoring (hums) to helicopter rotor, engine, and drive systems.” In: (cit. on p. 2).

Fancello, Matteo (2012). “A Co-Simulation Approach for Mixed Smooth and Nonsmooth Dynamics in Multibody Problems.” In: (cit. on p. 24).

Farrar, Charles R and Keith Worden (2000). “An introduction to structural health monitoring.” In: (cit. on p. 54).

Farrar, Charles R. and Keith Worden (2013). “Structural Health Monitoring.” In: (cit. on pp. 1, 5, 52, 53).

Figueiredo, Eloi, Gyuhae Park, Charles R Farrar, and Keith Worden (2010). “Machine learning algorithms for damage detection under operational and environmental variability.” In: (cit. on pp. 1, 10, 11, 64).

Flores, P, M Machado, M T Silva, and J M Martins (2011). “On the continuous contact force models for soft materials in multibody dynamics.” In: (cit. on p. 24).

Ghiringhelli, G L, P Masarati, and P Mantegazza (2000). “A multi-body implementation of finite volume beams.” In: (cit. on p. 47).

Gul, Mustafa and F Necati Catbas (2009). “Statistical pattern recognition for Structural Health Monitoring using time series modeling: Theory and experimental verifications.” In: (cit. on pp. 11, 12, 19, 37).

Hodges, D H and E H Dowell (1974). “Nonlinear Equation for the Elastic Bending and Torsion of Twisted Nonuniform Rotor Blades.” In: (cit. on p. 47).

Hunt, K H and F R E Crossley (1975). “Coefficient of restitution interpreted as damping in vibroimpact.” In: (cit. on p. 24).

Lankarani, Hamid M and Parviz E Nikravesh (1994). “Continuous contact force models for impact analysis in multibody systems.” In: (cit. on p. 24).

Mahalanobis, P C (1930). “On Tests and Meassures of Groups Divergence.” In: (cit. on p. 35).

McCulloch, Warren S and Walter H Pitts (1943). “A logical calculus of the ideas immanent in nervous activity.” In: (cit. on p. 51).

McLachlan, G J (1999). “Mahalanobis Distance.” In: (cit. on p. 35).

Penny, W and L Harrison (2006). “Multivariate autoregressive models.” In: (cit. on p. 32).

Rosenblatt, Frank (1957). “The perceptron: a perceiving and recognizing automaton.” In: (cit. on p. 52).

Ruotolo, R and C Surace (1999). “Using SVD to detect damage in structures with different operational conditions.” In: (cit. on pp. 13, 14, 55).

Santos, Adam, Eloi Figueiredo, M F M Silva, C S Sales, and J C W A Costa (2015). “Machine learning algorithms for damage detection: Kernel-based approaches.” In: (cit. on p. 11).

Serafini, Jacopo, Giovanni Bernardini, Roberto Porcelli, and Pierangelo Masarati (2018). “Rotor blade shape reconstruction from strain measurements.” In: (cit. on pp. 2, 48).

— (2019). “In-flight health monitoring of helicopter blades via differential analysis.” In: (cit. on pp. 8, 9, 29, 49).

Shabana, Ahmed A (2005). “Dynamics of Multibody Systems.” In: (cit. on pp. 3, 4).

Verne, J. (1957). *Journey to the Center of the Earth*. Classics illustrated. Huge Print Press. ISBN: 9780758311993 (cit. on p. 1).